FINAL REPORT

Project B2

October 2019

Evaluation of Work Zone Mobility by Utilizing Naturalistic Driving Study Data

Dr. Huaguo Hugo Zhou | Auburn University

Dan Xu, Ph.D. Student | Auburn University

Dr. Rod Turochy | Auburn University

STRIDE | Southeastern Transportation Research, Innovation, Development and Education Center

UF | Transportation Institute UNIVERSITY of FLORIDA

TECHNICAL REPORT DOCUMENTATION PAGE

1. Report No. Project B2	2. Government Accession No.	3. Recipient's Catalog No.
4. Title and Subtitle Evaluation of Work Zone Mobility by Utilizing Naturalistic Driving Study Data		**5. Report Date** October 2019 **6. Performing Organization Code**
7. Author(s) Dr. Huaguo Hugo Zhou, Ph.D., Auburn University Dan Xu, Ph.D., Auburn University Rod Turochy, Ph.D., Auburn University		**8. Performing Organization Report No.** STRIDE Project B2
9. Performing Organization Name and Address Auburn University 238 Harbert Engineering Center Auburn, AL 36849		**10. Work Unit No.** **11. Contract or Grant No.** Funding Agreement Number 69A355174710
12. Sponsoring Agency Name and Address University of Florida Transportation Institute Southeastern Transportation Research, Innovation, Development and Education Center 365 Weil Hall, P.O. Box 116580 Gainesville, FL 32611		**13. Type of Report and Period Covered** 8/15/2018 to 10/31/2019 **14. Sponsoring Agency Code**

15. Supplementary Notes

16. Abstract

The objective of this research is to evaluate work zone mobility by utilizing naturalistic driving study (NDS) data. More specifically, this one-year proof-of-concept project is to ascertain if the existing NDS work zone database can be reused to develop new (or update existing) capacity and traffic flow models for work zones. In this study, a comprehensive literature review was conducted to summarize the past study results on work zone capacity, work zone simulation models, and NDS application in work zone safety studies. It concluded that no past studies were found on application NDS data in relation to work zone mobility. The complimentary NDS data set was collected, including time-series data and forward-view videos, for a total of 420 baseline events and 256 safety-critical events. Forward-view video was reviewed to ensure that it is related to a work zone, which includes a lane or shoulder closure, the presence of barriers, the presence of construction equipment or workers, etc. Time-series data includes variables such as vehicle speed, acceleration, and pedal position at 0.1 s intervals. In addition, radar data and driver risk perceptions were collected for these events. Finally, researchers identified a total of 38 safety-critical events and 64 baseline trips for data analysis based on a set of criteria. Based on the sample size, the analysis focused on three types of freeway work zones (two-toone lane closure, two-to-two, and three-to-three shoulder closure). The fundamental traffic flow theory, Greenshield's model, and work zone capacity method in the Highway Capacity Manual (HCM) were applied to identify the speed-flow-density relationship for different work zone configurations. The time headway and space headway distributions were further analyzed with driver characteristics such as driver's gender, age group, risk perceptions. The results concluded that NDS data can be used to develop car-following models at work zones with consideration of driver population factor, which can be applied to improve work zone capacity methods and other work zone planning and simulation tools. Further study is recommended to collect more complete NDS trip data at different work zone configurations.

17. Key Words	18. Distribution Statement
Work Zone, Naturalistic Driving Study, Highway Capacity Manual, Traffic Flow Modeling, Driving Behavior	No restrictions to all.

19. Security Classif. (of this report)	20. Security Classif. (of this page)	21. No. of Pages	22. Price
		59 pages	

DISCLAIMER

The contents of this report reflect the views of the authors, who are responsible for the facts and the accuracy of the information presented herein. This document is disseminated in the interest of information exchange. The report is funded, partially or entirely, by a grant from the U.S. Department of Transportation's University Transportation Centers Program. However, the U.S. Government assumes no liability for the contents or use thereof.

ACKNOWLEDGEMENT OF SPONSORSHIP AND STAKEHOLDERS

This work was sponsored by a contract from the Southeastern Transportation Research, Innovation, Development and Education Center (STRIDE), a Regional University Transportation Center sponsored by a grant from the U.S. Department of Transportation's University Transportation Centers Program.

Funding Agreement Number - 69A3551747104

LIST OF AUTHORS

Lead PI:

Huaguo Hugo Zhou, Ph.D.
Auburn University
zhouhugo@auburn.edu
ORCID 0000-0001-5210-036X

Co-PI:

Rod Turochy, Ph.D.
Auburn University
rodturochy@auburn.edu
ORCID 0000-0003-2294-7388

Additional Researchers:

Dan Xu, Ph.D. Student
Auburn University
dzx0004@auburn.edu
ORCID 0000-0001-7501-3111

TABLE OF CONTENTS

LIST OF FIGURES

LIST OF TABLES

ABSTRACT

The objective of this research is to evaluate work zone mobility by utilizing naturalistic driving study (NDS) data. More specifically, this one-year proof-of-concept project is to ascertain if the existing NDS work zone database can be reused to develop new (or update existing) capacity and traffic flow models for work zones. In this study, a comprehensive literature review was conducted to summarize the past study results on work zone capacity, work zone simulation models, and NDS application in work zone safety studies. It concluded that no past studies were found on application NDS data in relation to work zone mobility. The complimentary NDS data set was collected, including time-series data and forward-view videos, for a total of 420 baseline events and 256 safety-critical events. Forward-view video was reviewed to ensure that it is related to a work zone, which includes a lane or shoulder closure, the presence of barriers, the presence of construction equipment or workers, etc. Time-series data includes variables such as vehicle speed, acceleration, and pedal position at 0.1 s intervals. In addition, radar data and driver risk perceptions were collected for these events. Finally, researchers identified a total of 38 safety-critical events and 64 baseline trips for data analysis based on a set of criteria. Based on the sample size, the analysis focused on three types of freeway work zones (two-to-one lane closure, two-to-two, and three-to-three shoulder closure). The fundamental traffic flow theory, Greenshield's model, and work zone capacity method in the *Highway Capacity Manual* (HCM) were applied to identify the speed-flow-density relationship for different work zone configurations. The time headway and space headway distributions were further analyzed with driver characteristics such as driver's gender, age group, risk perceptions. The results concluded that NDS data can be used to develop car-following models at work zones with consideration of driver population factor, which can be applied to improve work zone capacity methods and other work zone planning and simulation tools. Further study is recommended to collect more complete NDS trip data at different work zone configurations.

Keywords:

Work Zone, Naturalistic Driving Study, Highway Capacity Manual, Traffic Flow Modeling, Driving Behavior

EXECUTIVE SUMMARY

As maintenance and construction work increase, work zone mobility has become a major concern for transportation agencies. Most work zone mobility studies have mainly applied simulation-based, non-parametric, and parametric methods to estimate and predict work zone capacities without considering the driver characteristics. The naturalistic driving study (NDS) data offer a unique opportunity to observe actual work zone layouts, traffic conditions, and driver behaviors negotiating freeway work zones. Although there have been several work zone naturalistic driving studies, none of them have focused on the work zone mobility. This project utilized a part of a complimentary NDS data set (including 420 baseline events and 256 safety-critical events in total that have been collected for a previous work zone safety study). Based on specific criteria, a total of 38 safety-critical events and 64 baseline events were applied to evaluate capacity, car-following characteristics, and driver types in three freeway work zone configurations (two-to-one lane closure, two-to-two, and three-to-three shoulder closure configurations).

The key findings are summarized as follows:

- The linear relationship between speed and density was observed from work zone NDS data. The capacities predicted from NDS speed-flow regression models are typically greater than those from HCM estimation. The free flow speeds estimated from NDS speed-density regression models for Lane Closure (LC) 2-1, Shoulder Closure (SC) 2-2, and SC 3-3 are 62, 73, and 72 mph, respectively.
- From headway distribution, it was found that the headway decreases as the level of service (LOS) drops because, the more congested, the closer the vehicles will get. In addition, it was found that 85% of drivers selected their time headway from 0.8 to 2.8 s and 50 to 175 ft in space headway at work zones.
- The headway convergence of female drivers reveals that female drivers' headway selections are more consistent than male drivers', although the average time headway of male drivers (2.6 s) is greater than that of female drivers (2.0 s) based on the limited sample size.
- Senior drivers were found to choose longer time headway when passing a work zone. Young drivers age less than 24 appear to maintain 2.1 s time headway. The middle-aged drivers from 24 to 60 select their time headway as 2.4 s. The average time headway of senior drivers is the longest of 2.6 s.
- Based on the risk perception, female drivers seem to be more timid as their risk scores are higher than those of male drivers. Teen drivers younger than 24 were found to take more risks when driving, as their risk perceptions were the lowest among three age groups (≤24, 25-59, and ≥60).

Although the freeway work zone capacity methodology proposed in the latest edition of the HCM has been substantially improved over previous editions, it is still limited by the fact of the

macroscopic model, which cannot account for various work zone configurations. The results from the NDS data offer a unique opportunity to observe actual driver behaviors negotiating different work zone configurations, which can be utilized to improve the work zone capacity method defined by HCM and other work zone planning and simulation tools. For example, the preliminary results suggested that the capacities predicted by HCM are lower than that by NDS regression models, which implies the HCM might underestimate the work zone capacity or additional parameters (such as population factor), which should be included in HCM models. The results on headway selections by different types of drivers can also be applied to improve or calibrate work zone planning and simulation tools. More complete work zone NDS data that cover the entire work zone area should be collected to develop car-following models at work zones in the next phase.

1.0 INTRODUCTION

As the National Highway System (NHS) grows older, the increasing number of work zones has been presented to address the growing needs of maintenance and construction. However, reduced operating speeds, narrowed lane widths and shoulder clearances, along with other construction activities, not only result in crashes but also cause excessive delays (*1*). It has been well stated that the capacity per lane in the work zone is lower than that in the nonwork zone due to the reduced operating speed, lane width and shoulder clearance (*2*). Different passing behaviors along the work zone area can contribute to the loss of work zone capacity as well (*2*). According to the Federal Highway Administration (FHWA), work zones led to approximately 24% of the nonrecurring freeway delay, which was equivalent to about 888 million vehicle-hours in 2014 (*1*). Moreover, work zone activities occurred on roads that were often already congested, which brought more mobility issues on the busy arterials.

As a major concern of the work zone, there have been plenty of past studies focused on work zone capacity issues. Numerous statistical and simulation-based methods have been proposed to estimate or predict the work zone capacity (*2-8*). In the sixth edition of the *Highway Capacity Manual* (HCM), the new freeway work zone capacity model estimates work zone capacity as a function of the lane closure severity index, barrier type, area type, lateral clearances, and day- or nighttime work conditions (*5*). Meanwhile, microscopic traffic simulation models, such as CORSIM (University of Florida, USA) and VISSIM (Karlsruhe, Germany), have been applied to estimate and calibrate the operational capacity of work zones with different lane closure configurations (*7, 9-10*). In order to represent the increasingly complex freeway systems and freeway work zones, it suggested that further calibrations are needed to address other issues with specific work zone configurations (*2*). Although the speed–flow–density relationship has been widely used to estimate freeway capacity, only a few work zone capacity estimation methods were derived from speed–flow relationships (*3, 11*). Thus, more study is needed to derive work zone capacity from the speed–flow–density relationship to provide a reliable estimate.

Although the freeway work zone capacity methodology proposed in the latest edition of the HCM has been substantially improved over previous editions, it is still limited by the fact of the macroscopic model, which cannot account for various work zone configurations (*4*). The Naturalistic Driving Study (NDS) data collected by the second Strategic Highway Research Program (SHRP2) offers a unique opportunity to observe actual work zone layouts, traffic conditions, and driver behaviors negotiating freeway work zones (*12*). Vehicle speed, brake pedal use, deceleration/acceleration rates, and headways through the entire work zone can be quite valuable for gaining a deeper understanding of factors that affect work zone capacity. Three ongoing work zone projects utilize NDS data, but none of them aim to explore work zone mobility issues (*13-15*).

1.1 Objective

Based on the available complimentary data set, the objectives of the current study were set to:

1. Study the work zone traffic flows in different work zone configurations; and
2. Explore time and space headway distributions and their relation with driver characteristics.

1.2 Scope

The scope of the study was limited to work zones on Interstate highways. Using NDS data with time-series, forward roadway videos, radar data, and driver risk perceptions, the study investigated the work zone traffic flows in two-to-one lane closure, two-to-two, and three-to-three shoulder closure work zone configurations.

2.0 LITERATURE REVIEW

This section synthesizes relevant literature on the topic of estimating and predicting the freeway work zone capacity. A thorough literature review was conducted to assess the state of the practice in defining, modeling, and evaluating the freeway work zone mobility. Numerous studies have focused on work zone capacity issues, including a number of methods that have been proposed to estimate and predict work zone capacity. These methods can be divided into three categories, i.e., simulation-based, nonparametric, and parametric (*3*). The following sections summarize these methods and recent NDS studies related to work zones in the United States.

2.1 Simulation-Based Method

According to the use of traffic analysis tools and simulation models in the FHWA Traffic Analysis Toolbox, simulation tools have been widely applied in much traffic analysis research (*16*). Focused on different aspects, simulation tools can be grouped into four categories: sketch-planning tools, macroscopic simulation models, mesoscopic simulation model, and microscopic simulation models.

Sketch-planning methodologies and tools produce general order-of-magnitude estimates of travel demands and traffic operations in response to transportation changes (*17*). The planning level work zone simulation tools include software such as QUEWZ (University of Florida, USA), QuickZone (FHWA, USA), FREEVAL-WZ (North Carolina, USA), etc. (*18*). As high-level planning applications, these deterministic tools aid in simpler approaches in that data requirements, calibration, and interpretation of the results are highly aggregated. Thus, they cost the least time or money in which to facilitate rapid analysis. These advantages, however, are coupled with the weakness in that the network complexity, potential network impacts, vehicle interactions, and high-level analysis are limited. It was found that the QUEWZ and QuickZone were not accurate in past studies (*19-20*). Research conducted by Benekohal et al. stated that QUEWZ overestimated the capacity and average speed; further, the queue length from QuickZone did not match the field data (*19*). Ramezani and Benekohal also reported that the maximum queue length was overestimated by these tools (*20*). The inaccurate results were caused because QUEWZ and QuickZone applied outdated HCM methodology to estimate performance measures in work zones. For example, the QUEWZ models were developed based on the 1965 HCM general speed-flow relationship and regression based on field data (*21*). Although the FREEVAL-WZ applied the latest methodology of 2016 HCM and is able to model different work zone scenarios as well as quantify the effects of congested periods over time and space (*22*), its effectiveness has not been fully explored.

Macroscopic simulation models are based on the deterministic relationships of the flow, speed, and density of the traffic stream that treat traffic flows as an aggregate quantity

without analyzing individual vehicle movement (*17*). These simulation models include software such as the TRANSYT-7F (University of Florida, USA) package within the *Highway Capacity Software* from McTrans (*18*). While these models have the ability to model a large geographic area and provide slightly more details than the sketch-planning tools, they are still limited to their simple representation of traffic movement and are unaccounted for the stochasticity of work zone environments.

Mesoscopic simulation models are a combination of both microscopic and macroscopic simulation models (*17*). While they still model at an aggregate level and the focus is on the movement of a platoon of vehicles, their unit of traffic flow is the individual vehicle; further, different platoons' interactions are considered. One example of mesoscopic simulation software is DYNASMART-P (University of Florida, USA), developed by McTrans in 2007 (*18*). It provides the capability to model the evolution of traffic flows in a traffic network when individual travelers can make decisions on selecting the best path (*23*). These models are able to model both large geographic areas and corridors, but their primary limitation is their inability to model detailed operational strategies. Thus, these tools may not be helpful for individual work zones.

Microscopic models simulate the movement of every vehicle in the network based on car-following, lane-changing, and gap-acceptance theories (*17*). These tools are based on a stochastic process, and every vehicle in the network can be tracked over short time-intervals so that the result of each run is unique. Popular microscopic simulation software includes CORSIM and VISSIM, which are developed by FHWA and the PTV Group, respectively (*18*). These models aim to represent transportation systems accurately at the individual vehicle level and are effective in modeling plenty of scenarios such as heavily congested conditions, complex geometric configurations, and system-level improvement impacts. CORSIM and VISSIM have been used in several studies to estimate the capacity of work zones with different lane closure configurations (*7, 9-10*). However, a detailed and comprehensive analysis requires a substantial amount of roadway geometry, traffic control, and traffic pattern data. In addition, to represent real-world traffic conditions, it was suggested that further calibration work is needed to address other issues with specific work zone configurations (*2*). This calibration process is usually tedious and expensive.

2.2 Nonparametric Method

When estimating the work zone capacity, sometimes it is not feasible to describe the capacity by mathematical functions due to nonlinear relationships and complex interactions between a large number of variables and capacity (*24*). Therefore, several non-parametric methods, such as neural-fuzzy logic, decision tree, and ensemble tree models, have been applied to provide work zone capacity estimations (*3*). The nonparametric method is a technique that does not assume that the structure of a model is fixed (*25*). Because of fewer assumptions being made by nonparametric

methods, these models are more flexible, robust, and applicable to nonquantitative data (*26*). However, it was also pointed out that nonparametric approaches typically require generous historical traffic data to provide accurate and reliable predictions (*28*).

The neural-fuzzy logic method was the first nonparametric method applied to estimate the work zone capacity (*24*). The study introduced a novel adaptive neuro-fuzzy logic model, including 17 different factors that have an impact on the work zone capacity. The authors concluded that this model can provide a more accurate estimate, compared with two empirical equations. However, due to its complexity, the model was hardly applicable to the users. In another study, Karim and Adeli proposed a radial-basis function neural network model, which considered 11 parameters to learn the mapping from quantifiable and nonquantifiable factors in the estimation of work zone capacity (*28*). In 2011, a decision-tree-based model was developed to provide a higher estimation accuracy of the work zone capacity (*4*). This model considered 16 influencing factors; in addition, the data in this study were collected from 14 states. The results demonstrated that this model outperformed the neural-fuzzy approach, as it predicted more accurately; further, it was applicable to all users. The weakness of this method is that the tree structure is highly dependent on the training and testing data. In other words, a slight change in the training and testing data set will dramatically alter the results. In order to address this weakness, an ensemble tree method was applied in another research (*6*). Weng and Meng built an ensemble tree consisted of 105 individual decision trees by using a bootstrap aggregation method. It proved that the ensemble tree was more accurate and stable than the decision tree method. However, due to the absence of graphical-display results, it was complicated to understand the detailed relationship between the capacity and factors. In addition, the decision tree and ensemble tree both discretize the continuous factors based on the *F*-test to make them categorical when building the tree structure. This process may lower the accuracy of the entire work (*29*).

2.3 Parametric Method

Many studies have used the parametric method to estimate work zone capacity. This method uses a predetermined form to predict work zone capacity based on the field data so that the coefficients of predictors can be determined (*27*).

In 1994, Krammes and Lopez developed a multiregression model to estimate the short-term work zone capacity based on the data collected in 33 work zones in Texas (*30*). It only included parameters such as work intensity, presence of ramps, and heavy vehicle adjustment factor. Therefore, Kim et al. proposed another multiregression model that considered more capacity-influencing factors for short-term work zones, including the number of closed lanes, lane closure locations, heavy vehicle percentage, lateral distance to the lane closure, work zone length, work intensity, and the work zone grade (*31*). As for long-term work zones, a generic multiplicative model was proposed to

investigate capacity with lane closure conditions in Ontario, Canada (*32-33*). The variables included in the model are temporal variations, grade, day of week, and weather conditions, which were found to have significant impacts on the long-term work zone capacity.

In addition, the sixth edition of the HCM offered detailed guidance on determining work zone capacity. It defined the capacity as "the maximum sustainable hourly flow rate at which persons or vehicles reasonably can be expected to traverse a point or a uniform section of a lane or roadway during a given time period under the prevailing roadway, environmental, traffic, and control conditions" (*5*). Upon the work zone capacity, Yoem et al. performed an extensive literature search, established a relationship between the queue discharge rate (QDR) and pre-breakdown capacity (PBC), and provided a regression model for estimating work zone capacity under different conditions (*2*). This work, currently included in the sixth edition of the HCM, was based on 90 archival literature sources and 12 data sets collected from the field. It stated that freeway work capacity corresponds to the maximum sustainable flow rate immediately preceding a breakdown, which is the PBC (*5*). However, it is not feasible to measure the pre-breakdown value in the work zone. Thus, the HCM proposed a method to calculate the QDR first, which can be easily measured via video cameras or other data collection tools, and then converted the QDR to the corresponding PBC by using a conversion ratio. The QDR is calculated as follows:

$$QDR_{WZ} = 2,093 - 154 \times LCSI - 194 \times f_{Br} - 179 \times f_{AT} + 9 \times f_{LAT} - 59 \times f_{DN} \quad \text{EQUATION 1}$$

where

QDR_{WZ} = the average 15-min queue discharge rate at the work zone bottleneck;

$LCSI$ = lane closure severity index;

f_{Br} = indicator variable for barrier type (0 for concrete; 1 for cone or drum);

f_{AT} = indicator factor for area type (0 for urban; 1 for rural);

f_{LAT} = lateral distance from the edge of travel lane adjacent to the work zone to the barrier, barricades, or cones (0-12 ft); and

f_{DN} = indicator variable for daylight or night (0 for daylight; 1 for night).

The lane closure severity index is illustrated in Exhibit 10-15 in the HCM. It also applies to shoulder closures without lane closures. This index is calculated as follows:

$$LCSI = \frac{1}{OR \times N_O} \quad \text{EQUATION 2}$$

where

$LCSI$ = lane closure severity index;

OR = open ratio, the ratio of the number of open lanes during road work to the total (or normal) number of lanes (decimal); and

N_O = number of open lanes in the work zone.

After obtaining the QDR, the PBC can be calculated as follows:

$$C_{WZ} = \frac{QDR_{WZ}}{100 - a_{WZ}} \times 100 \qquad \text{EQUATION 3}$$

where

C_{WZ} = pre-breakdown flow rate; and

a_{WZ} = percentage drop in prebreakdown capacity at the work zone due to queuing conditions (%), an average value of 13.4% in freeway work zones.

Another way to estimate the work zone capacity is to derive the capacity from speed-flow curves. Over the years, some researchers adopted this method to derive information from the prediction model (*3, 11, 34-36*). For example, Benekohal et al. presented a step-by-step methodology to estimate the operating speed and capacity on lane closure two-to-one work zones in Illinois (*37*). The authors recorded 30 hours of video data from 11 work zones on the Interstate and compared the field data with predictions for validation. In this study, the operating speed was modeled as a function of work intensity, lane width, lateral clearance, and other factors to examine the influences of external factors on traffic speed. Sarasua et al. conducted a study to develop the speed-flow curves for lane closure in two-to-one, three-to-two, and three-to-one work zones (*11*). The authors revealed that passenger car equivalents (PCEs) differed for various speed ranges, and PCEs for various speed groups are recommended in calculating capacity. Racha et al. collected field data from 22 work zones in South Carolina and modeled the work zone capacity from the relationships among speed, flow, and density (*34*). The authors also demonstrated that a non-linear hyperbolic model was developed to depict the speed-density relationship for two-to-one lane closure configurations of Interstate highway work zones. Avrenli et al. examined the speed-flow relationship of work zones with no lane closure (*35*). These authors developed two nonlinear models for work zones with no lane closure under uncongested and congested conditions. It was found that the flow rate of the free-flow regime was much lower than the capacity that the HCM 2000 model predicted.

2.4 Other Work Zone Naturalistic Driving Studies in the United States

Field data and traffic simulation tools have been used to develop the freeway work zone capacity model. However, the NDS data collected by the SHRP2 offers a unique opportunity for a first-hand forward-view of an actual driver on work zone temporary

traffic control layout and breakdown conditions, which can help determine how drivers navigate through different work zones under different traffic flow conditions (*12*).

So far, there are three work zone projects utilizing NDS data sponsored by the United States Department of Transportation (USDOT), but none of them aims to explore work zone mobility issues (*13-15*). The Iowa State University is using NDS data to investigate work zone safety, especially the role of speed and distraction in work zone crashes and near-crashes (*13*). Researchers from the University of Missouri have been conducting a study to predict the occurrence of a safety-critical event in work zones by using pre-event variables from NDS data (*14*). Further, the third work zone study used statistical descriptions of normal driving behavior to identify abnormal behavior as the basis for countermeasures by utilizing NDS data (*15*).

In addition, there are also other work zone naturalistic driving studies, but their focuses are on safety analysis. Bharadwaj et al., for example, investigated risk factors and developed a binary logistic regression model to estimate the crash risk in work zones (*38*). The authors also quantified the risk of different contributing factors. For instance, it was found that the odds ratio of driver inattention is 29, which is the most critical behavioral factor contributing to crashes. Chang and Edara applied four machine-learning algorithms to work zone events with NDS data to predict the occurrence of a safety-critical event by using pre-event variables (*39*). These algorithms included the random forest, deep neural network, multilayer feed forward neural network, and t-distributed stochastic neighbor embedding. It was concluded that the random forest algorithm performed the best in classifying different safety-critical events with a prediction accuracy of 97.7%. In another machine learning research, Abodo et al. developed a video analytics software application to detect work zones in the NDS data (*40*). This application tied the NDS video content to geolocations and other trip attributes into the Roadway Information Database (RID), accurately and exhaustively. The authors also stated that their future work will expand the capabilities of the application to apply to weather events and traffic signal state.

2.5 Discussion of Literature Review Findings

The comprehensive review of available literature conducted in this study indicated that, to the best of our knowledge, no NDS studies have focused on work zone traffic flow modeling and capacity estimation. In addition, although the speed-flow relationship has been widely adopted to estimate the freeway capacity, only a few studies used this method to analyze work zone capacity on the freeways. Furthermore, none of the work zone capacity studies in the past considered driver population factors and their car-following behaviors. The NDS can provide driver characteristics such as risk perceptions and crash history. The driver types and their headway selections in the work zone would be helpful to identify how driver behaviors affect work zone capacity. Thus, the results

from NDS data can be used to enhance the work zone capacity model by adding additional parameters such as population factors.

3.0 DATA DESCRIPTION

SHRP 2 NDS data involves 3,147 drivers collected from the year 2010 to 2012 in six states: New York, Pennsylvania, Florida, Washington, North Carolina, and Indiana. The collected event data contains baseline events and safety-critical events. Each event was coupled with a brief video clip of the forward roadway with a time-series report, which includes selected vehicle kinematics such as speed (kmph), acceleration/deceleration rate (*g*), brake status (0 or 1), gas pedal position (0-100), etc. The following sections describe the collected data, the data reduction procedure, and the limitations of the final data set.

3.1 Data Collection

The original data set was obtained complimentarily from an on-going project: *Evaluation of Work Zone Safety Using the SHRP 2 Naturalistic Driving Study Data* (identified as doi:10.15787/VTT1TG6S). Typically, a three-step method can be used to collect NDS data from the SHRP2 NDS data set. First, a data request needs to be prepared and sent to the Virginia Tech Transportation Institute (VTTI) to extract the specific data set. Second, approval from the Institutional Review Board (IRB) needs to be secured. Last, the data set will be delivered and extracted for analysis.

A total of 420 baseline events and 256 safety-critical events was received. The time-series data (i.e., speed, acceleration/deceleration rate, pedal status, and position, etc.) and video clips of the forward roadway were also obtained. The following two figures present examples of time-series data and a video frame of the forward-view. As highlighted in Figure 1, “vtti.accel_x” is the vehicle acceleration in the longitudinal direction versus time with the unit of *g*. “pedal_brake_state” is the on or off press of a brake pedal with “0” (off press) or “1” (on press). “pedal_gas_position” is the position of the accelerator pedal collected from the vehicle network and normalized using manufacturer specs ranging from zero to 100. “speed_network” is the vehicle speed indicated on speedometer collected from the network with the unit of kmph. All the time-series data were collected at 0.1 s intervals. The video can also be linked to time-series data so that the corresponding speed, acceleration/deceleration rate, pedal status, and positions at such 0.1 s can be obtained. This linkage is based on the “timestamp”. For example, the “timestamp” on the forward-view video frame is “5127613” as shown in Figure 2. This number is included in “vtti_timestamp” of the time-series spreadsheet. Thus, time-series and forward-view videos can be reviewed together.

System	vtti.time	vtti.file_id	vtti.accel_x	vtti.pedal_brake_state	vtti.pedal_gas_position	vtti.speed_gps	vtti.speed_network
1	366905	86546163					
2	367000	86546163	0.0051	0	19.530001		117
3	367100	86546163	0.008	0	19.530001		117
4	367200	86546163	0.0022	0	19.530001		117
5	367299	86546163	0.0138	0	19.530001		117
6	367400	86546163	0.0051	0	19.530001		117
7	367500	86546163	-0.0065	0	19.530001	114.110383	117
8	367600	86546163	-0.0152	0	19.530001		117
9	367699	86546163	0.0138	0	19.530001		117
10	367800	86546163	0.0167	0	19.530001		117
11	367899	86546163	0.0109	0	19.530001		117
12	368000	86546163	0.0167	0	19.530001		117
13	368099	86546163	0.0109	0	19.530001		117
14	368200	86546163	0.008	0	19.530001		117
15	368299	86546163	-0.0007	0	19.530001		117
16	368400	86546163	0.008	0	19.530001		117
17	368500	86546163	0.0022	0	19.530001	114.702972	117
18	368600	86546163	0.008	0	19.530001		117
19	368700	86546163	0.008	0	19.530001		117
20	368800	86546163	0.0167	0	19.530001		117

FIGURE 1. EXAMPLE TIME-SERIES DATA

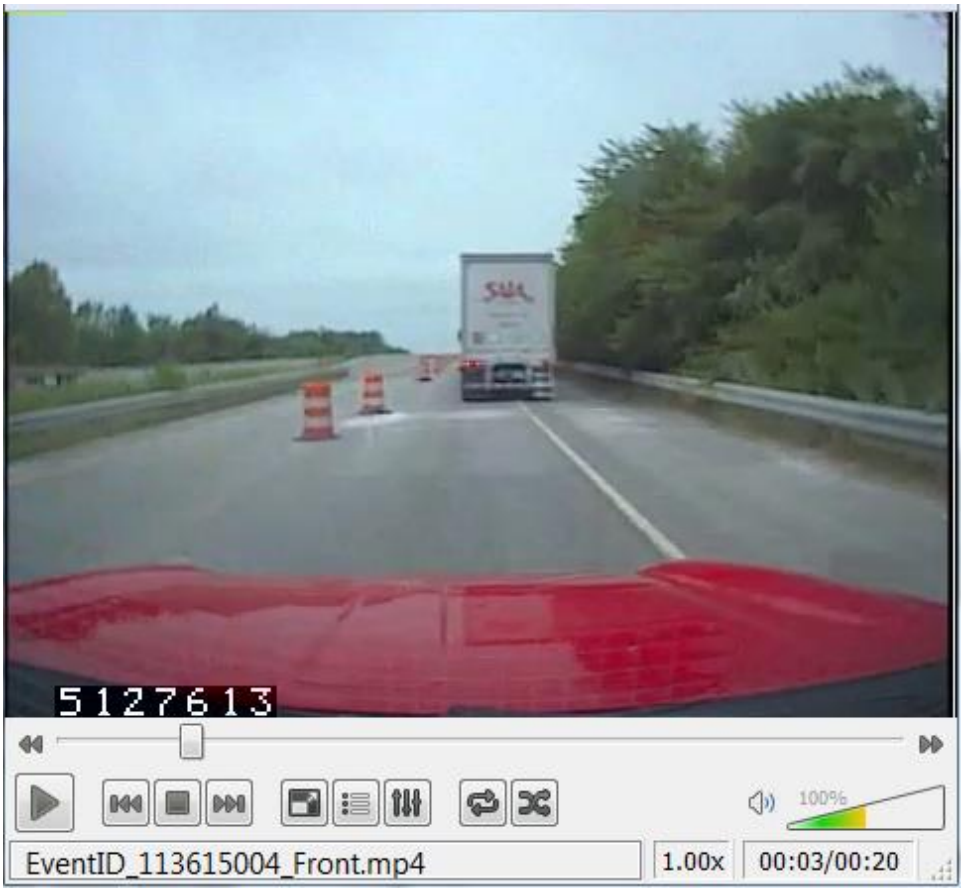

FIGURE 2. EXAMPLE FORWARD-VIEW VIDEO FRAME

In addition, baseline events are typically 21 s long and were randomly selected by VTTI. Safety-critical events include three types based on the outcome of events: crash, near-crash, and crash-relevant. For safety-critical events, the duration of each trip is 30 s.

Except for the existing data set from the project, as previously mentioned, additional data were also requested from VTTI. For example, in order to apply the speed-flow relationship, the radar data, including time headway (s), were required from VTTI. From the radar data dictionary file, the headway equals the distance between target and participant vehicle's front bumper divided by the participant's vehicle speed. In addition, the driver risk perception questionnaire was also requested. Driver risk perceptions were calculated based on self-reported measures, where driving indicated their perceptions of risk associated with different driving behaviors. The score ranges from 32 to 224. Higher scores indicate greater risk perceptions; therefore, these drivers tend to be cautious and obedient to traffic rules. Examples of radar data and driver risk perception questionnaires are demonstrated in Figures 3 and 4.

Syste	vtti.time	vtti.file_id	TRACK1_TARGET_TRAVEL_DIRECTION	TRACK1_LANE	TRACK1_IS_LEAD_VEHICLE	TRACK1_HEADWAY
1	165600	83035541	2	0	1	3.584804
2	165700	83035541	2	0	1	3.553329
3	165800	83035541	2	0	1	3.537469
4	165900	83035541	2	0	1	3.521509
5	166000	83035541	2	0	1	3.529881
6	166100	83035541	2	0	1	3.484506
7	166200	83035541	2	0	1	3.467442
8	166300	83035541	2	0	1	3.464281
9	166400	83035541	2	0	1	3.448081
10	166500	83035541	2	0	1	3.43198
11	166600	83035541	2	0	1	3.439541
12	166700	83035541	2	0	1	3.422906
13	166800	83035541	2	0	1	3.406207
14	166900	83035541	2	0	1	3.372728
15	167000	83035541	2	0	1	3.35586
16	167100	83035541	2	0	1	3.33999
17	167200	83035541	2	0	1	3.357758
18	167300	83035541	2	0	1	3.325972
19	167400	83035541	2	0	1	3.308162
20	167500	83035541	2	0	1	3.290187

FIGURE 3. EXAMPLE RADAR DATA

anonymousParticipantID	Red Light	Drving Sleepy	Risk for Fun	Sudden Lane Changes	Running Stop Sign	Speeding for Thrill	Failure to Yield
559722	7	6	7	6	7	7	7
946363	7	6	7	7	6	7	6
833451	5	5	4	4	6	4	3
540149	7	7	7	7	7	7	7
171437	7	6	7	6	7	7	7
820518	6	6	7	5	7	6	6
218891	7	7	5	6	4	6	7
229540	5	7	7	5	5	6	6
119136	4	4	7	4	7	7	6
861870	7	6	7	5	7	7	5
322943	7	6	7	6	5	7	5
927794	7	7	7	6	7	7	6
815989	7	7	7	6	7	7	7
386739	7	6	7	4	5	7	7
407125	7	7	7	7	7	7	7
287035	7	7	7	5	7	7	7
328645	7	7	7	7	7	7	7
201115	7	7	7	7	1	7	7
259960	7	5	7	4	7	6	5
765760	7	7	6	3	7	7	4

FIGURE 4. EXAMPLE DRIVER RISK PERCEPTION QUESTIONNAIRE

Furthermore, to compare the results from the HCM method and NDS data, several variables used to estimate the work zone capacity in the HCM model were manually collected from the forward-view video. The collected variables include the work zone type (i.e., lane closure or shoulder closure), number of closed lanes, type of barriers (i.e., concrete, cone, or drum), area type (i.e., urban or rural), lateral clearance from the edge of the travel lane adjacent to the work zone to the barrier (0-12 ft), and lighting conditions (i.e., daylight or night). These variables were coded in the time-series report and event detail table. The capacity of every event location was calculated.

3.2 Data Reduction

The original data includes trips traversing work zones from nine localities: business and industrial, bypass, church, interstate, moderate residential, open residential, playground, school, and urban. In this study, the focus is on the freeway work zone capacity estimation. Thus, only trips from Interstates were selected. To ensure that the event was related to a work zone, every forward roadway video was reviewed to confirm whether it was actually work zone related. The trips with lane closure conditions, the presence of barriers near the lane edge, the presence of construction equipment or workers, etc. were considered as the work-zone-related events, which were selected for further analysis. In addition, some trips have merging or diverging behaviors near the interchange. These movements increase the potential of conflicts and have an impact on capacity (*41*). Thus, trips with the merging or diverging behaviors were filtered from the data set. It was also found that lane-changing behaviors have a substantial impact on the traffic breakdown or capacity drop (*42-43*). Therefore, in this project, the events with lane-changing behaviors were removed. Lastly, events that did

not come with or missed a portion of time-series data, radar data, or driver risk perceptions were removed from the data set.

As a result, the final data set contains 38 safety-critical events and 64 baseline events. Details of the final data set are presented in Table 1, including work zone configurations, level of service (LOS), and a number of events. There are ten work zone configurations in total, including five lane closure and five shoulder closure configurations. The lane closure 2-1 indicates the one-lane closure at a two-lane work zone roadway. Similarly, the shoulder closure 2-2 means the shoulder closure at a two-lane work zone roadway. Due to limited sample size, the emphasized work zone configurations (e.g. Lane Closure 2-1, Shoulder Closure 2-2, and 3-3) were selected for further analysis. The LOS has seven categories from A1 to F. While LOS A1 indicates free flow with no lead traffic and LOS A2 is free flow with leading traffic present, the LOS B to F have the same definition as defined in HCM (*5*).

TABLE 1. DETAILS OF FINAL DATA SET

Work Zone Configurations		**Critical Events**							**Baseline Events**							**Total**
		LOS							LOS							
		A1	A2	B	C	D	E	F	A1	A2	B	C	D	E	F	
Lane Closure	**2-1**		**2**	**3**	**2**	**1**				**4**	**3**	**4**	**1**			**20**
	3-2			1		1				3	1					6
	3-1									1						1
	4-3			1												1
	4-2								1							1
Shoulder Closure	1-1				1					1	3					5
	2-2			**4**		**2**	**1**			**7**	**9**	**1**				**24**
	3-3		**1**	**4**	**4**	**4**			**1**	**6**	**9**	**3**				**32**
	4-4			2	2	2				2	2		1			11
	5-5										1					1

3.3 Limitations

One major limitation of the complimentary data is that both baseline and safety-critical events did not include a full driving trace through the entire work zone. A typical trip includes one of the following: 1) segment upstream of the work zone; 2) a short segment upstream and a short section within the work zone; 3) a segment within the work zone; and 4) a short segment within and downstream of the work zone. As a result, many events did not include much within work zone driving, and there was no trip that contained drivers entering and driving through the entire work zone. In addition, all events were from different locations. In other words, only one trip occurred at one specific location.

The other limitations are summarized below:

- Small sample size: 38 safety-critical events and 64 baseline events.
- Both critical and baseline events were sampled for a random 30 or 21 s trips, which did not cover the entire work zone.
- There are few trips at LOS E or LOS F. without them, it is challenging to model the work zone breakdown conditions.
- Radar data (time headway) is not available for some trips.

Due to limitations of the complimentary data set, the traffic flow and headway distribution on the freeway work zone were explored based on the available data for the limited number of work zone configurations.

4.0 METHODOLOGY

This section discusses the methods to perform the freeway work zone traffic flow modeling and headway distribution analysis.

4.1 Traffic Flow Modeling

The first step of the data analysis was to perform the speed-flow-density distribution from the time-series report and radar data. Speeds from speedometer were included in time-series. The flow rate could be determined by the time headway from radar data, and the density was then calculated by the time headway and speed. Consequently, the flow rate was determined by speed and density. From LOS A to F, all trips were analyzed for both shoulder closure and lane closure work zones.

4.1.1 Fundamental Traffic Flow Theory

The traffic flow theory studies the dynamic properties of traffic on-road sections. The fundamental traffic parameters are speed, flow, and density (*44*). The speed u is defined as the rate of motion in distance per unit of time (*44*). As provided in the NDS time-series report, the speed data collected from speedometer in kilometer per hour (kmph) is converted to the unit of miles per hour (mph). The flow q is defined as the number of vehicles that pass a point on a highway or a given lane or direction of highway during a specific time interval (*44*). Thus, the flow can be related to time headway as follows:

$$q = \frac{1}{h} \qquad \text{EQUATION 4}$$

where

q = flow in vehicle per hour (vph); and

h = time headway in hour per vehicle (hpv).

The density k is defined as the number of vehicles occupying a given length of highway or lane (*44*). It can be calculated by space headway as:

$$k = \frac{1}{s} \qquad \text{EQUATION 5}$$

where

k = density in vehicle per mile (vpm); and

s = space headway in mile per vehicle (mpv).

The space headway can be determined by speed and time headway as below:

$$s = u \times h \qquad \text{Equation 6}$$

When substituting Equations 5 and 6 in Equation 4, the equation will be:

$$q = u \times k$$ **Equation 7**

After plotting speed against calculated density, the relationship between speed and density in the NDS data seems to be linear. Thus, Greenshield's Model was then applied to model the traffic flows in work zones. The assumption of this model is that the speed and density are linearly related under uninterrupted flow conditions. This relationship is expressed mathematically and graphically below:

$$\boldsymbol{u = u_f - \frac{u_f}{k_j} \times k}$$ **EQUATION 8**

where

u_f = free flow speed; and

k_j = jam density.

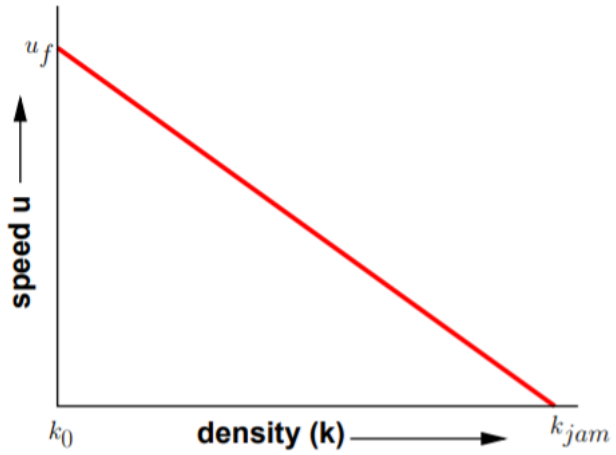

FIGURE 5. RELATIONSHIP BETWEEN SPEED AND DENSITY (45)

This equation indicates that the speed approaches free-flow speed when density closes to zero. These two parameters can be determined through field observations; further, the NDS can provide this information. Then, the relation with the flow and speed can be derived from Equations 7 and 8:

$$\boldsymbol{q = k_j \times u - \frac{k_j}{u_f} \times u^2}$$ **EQUATION 9**

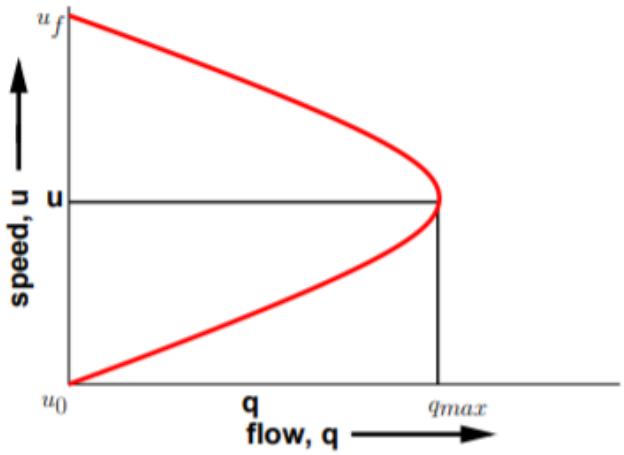

FIGURE 6. RELATIONSHIP BETWEEN SPEED AND FLOW (45)

4.1.2 HCM Model

As aforementioned in the literature review, it was proposed that the freeway work zone capacity should be estimated in terms of QDR and then converted to PBC if desired by using a default conversion factor of +13.4% for freeways (*5*). The predictive model for freeway work zone QDR is a function of the work zone configuration and other prevailing conditions, as illustrated in Equation 1, including lane closure severity index, barrier type, area type, lateral clearances, and day- or nighttime work conditions. After collecting all the required data from NDS forward-view videos, the calculated QDR was converted back to PBC as demonstrated in Equation 3, which is the work zone capacity corresponding to the maximum sustainable flow rate immediately preceding a breakdown.

4.2 Headway Distribution

The time and space headway distribution in the freeway work zone traffic flow was explored under different work zone configurations. Time headway or headway is defined as the time between two consecutive vehicles (in seconds) when they pass a single point on a roadway (*46*). As the radar data dictionary file stated, the headway collected from radar equals to the distance between target and participant vehicle front bumper divided by the participant's vehicle speed. Thus, an average vehicle length of 25 ft (*47*) was added to such distance, so that the time headway was counted from the target vehicle's front bumper to the participant vehicle's front bumper. Space headway is defined as the distance between the same points of two consecutive vehicles following each other (*46*). Similarly, the space headway was calculated by the time headway and speed plus the vehicle length of 25 ft (*47*) per space headway definition.

It should be noted that the radar utilized in the NDS data collection can track eight objectives at the same time. Therefore, it is critical to ensure that the tracked objective is the target vehicle in front of the participant vehicle. Three parameters are required to

make this confirmation, as highlighted in Figure 3, including the travel direction of the target, the lane that the target used, and whether the target was the lead vehicle. In the parameter "TARGET_TRAVEL_DIRECTION," there are six indicators in which "2" indicates that the target was traveling in the same direction as the participant vehicle at the time t_i. "0" in the parameter of "LANE" represents the target was in the same lane as the participant vehicle. Last, "1" in "IS_LEAD_VEHICLE" means the target was the lead vehicle, and the target was the closest target that was in the same lane as the participant vehicle. Thus, after the procedure to ensure the headway data include the target vehicle in front of the participant vehicle with "2", "0", and "1", the headway in seconds was extracted to obtain further analysis.

In addition to the radar data that provide the time headway, this NDS data set also includes an addendum export file, which links the driver's background and vehicle's condition to the events that traversed freeway work zones. The driver's background contains gender, age group, education, work status, income, driver mileage last year, average annual mileage, years driving, number of violations, violation types, number of crashes, and the severity of each crash. The vehicle condition includes insurance status, vehicle classification, manufacture, model, and vehicle width. These two types of information are important to understand a driver's behavior in selecting his or her desired headway. All available trips were analyzed for both shoulder closure and lane closure work zones.

The driver risk perception was collected from the questionnaire designed to gauge the participant's perception of dangerous or unsafe driving behaviors or scenarios (*48*). This questionnaire includes 32 driving-behavior-related questions. For example, how would the participant evaluate the risk when not yielding the right of way, the participant's associated risk with passing other cars on the right side or on the shoulder of the road, the participant's associated risk with turning without signaling, etc. Each question was assigned a score from 1 (No Greater Risk) to 7 (Much Greater Risk); thus, a higher score indicates that the driver is more cautious or obedient to traffic rules. The total risk perception score of drivers is the sum of all the scores from questions in the questionnaire, which is an important factor to explore in regard to driver behaviors and characteristics. Finally, the relationships among driver risk perception, headway selection, driver characteristics, etc. were identified.

5.0 RESULTS

This section describes how the data from NDS outlined in Data Description led to the traffic flow modeling, and the comparison of results from the fundamental traffic flow theory and HCM method will be presented. First, the work zone traffic flows in work zone lane closure and shoulder closure configurations will be studied. Second, the time and space headway distributions at different LOS and their relationships with driver characteristics will be explored.

5.1 Traffic Flow Modeling

After data cleaning, the final data set contains 38 safety-critical events and 64 baseline events. There are ten work zone configurations, including five lane closure and five shoulder closure configurations among all the events/trips. Due to the small sample size, only the work zone configurations with more than 20 trips were extracted for further analysis. As highlighted in Table 1, the analyzed work zone configurations were Lane Closure (LC) 2-1 and Shoulder Closure (SC) 2-2 and 3-3. Fundamental traffic flow theory was applied to model traffic flow in work zones, and the HCM method was used to estimate the capacity for every work zone.

5.1.1 Lane Closure

Among the five lane closure configurations (e.g., LC 2-1, 3-2, 3-1, 4-3, 4-2), only lane closure 2-1 has 20 trips. It should be noted that those 20 trips were from 20 different LC 2-1 locations. The lane closure speed-density plots calculated from fundamental traffic flow theory and speed-flow estimation based on Greenshield's model are presented in Figures 7 and 8, respectively, which show the approximately linear relationship of speed and density in the two-to-one lane closure work zone. In Figure 7, the *x*-axis is the density (vpmpl) and the *y*-axis is the speed (mph). The navy-blue dots are the speed data from SHRP 2 NDS time-series reports and calculated density by applying fundamental traffic flow theory, including 20 traversals. The orange trend line is the linear regressions of calculated speed-density relationships from NDS data. The regression equation shows that the free flow speed is 62 mph and the jam density is 219 vpmpl. The R^2 for the NDS regression model is 0.5746, indicating that the data do not fit the model particularly well. However, from a review of data distribution, the linear relationship between speed and density is still observed. Due to the limited number of trips at LOS D and E, the predicted jam density may be overestimated. This may result in an overestimated capacity.

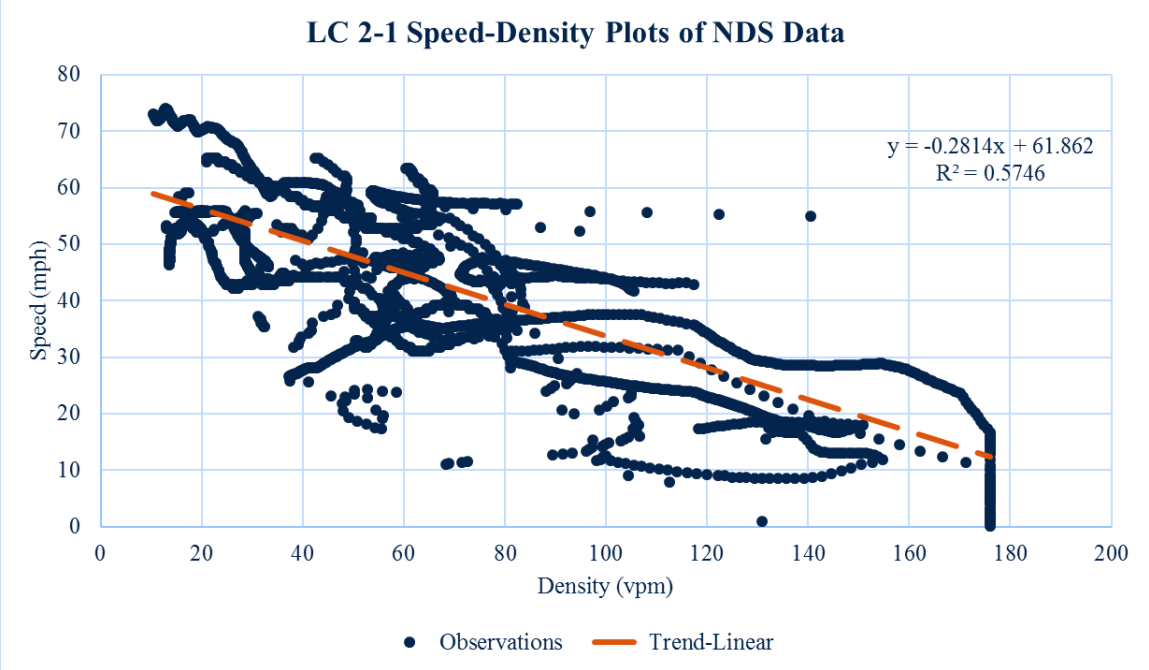

FIGURE 7. LANE CLOSURE 2-1 SPEED-DENSITY PLOTS

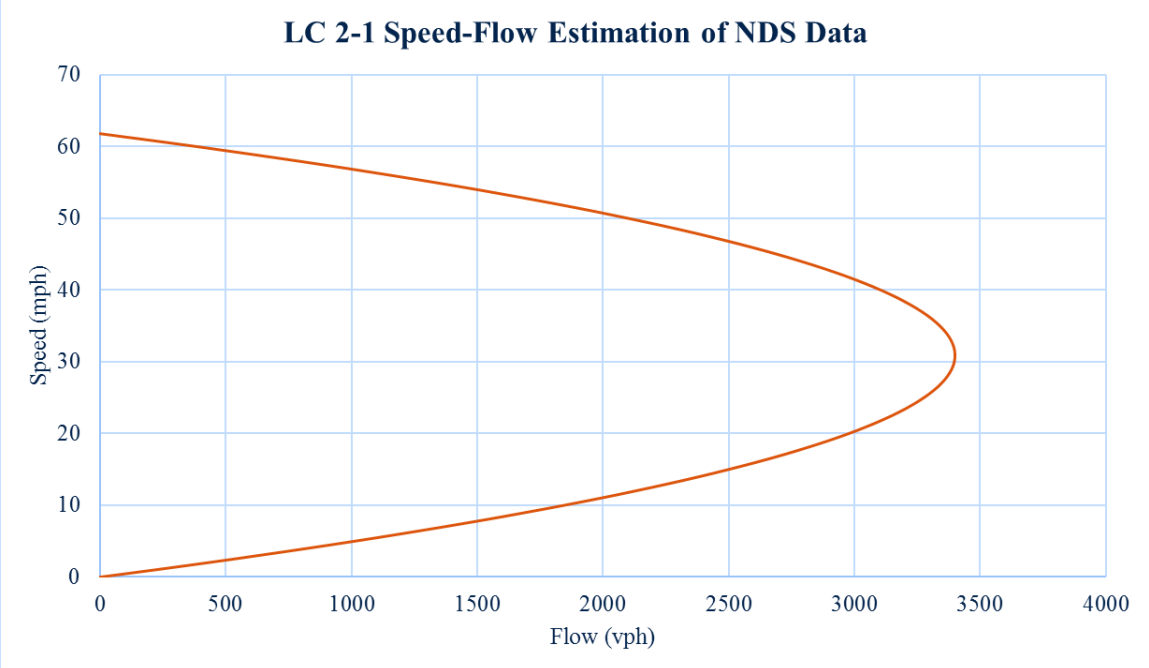

FIGURE 8. LANE CLOSURE 2-1 SPEED-FLOW ESTIMATION

In Figure 8, the orange line is the estimated flow based on the linear speed-density relationship. The estimated capacity of the two-to-one lane closure work zone is 3400 vphpl. The capacity estimation was also performed by using the HCM method as summarized in Table 2 for LC 2-1 work zone configuration.

Because every event was from a different location, the parameters observed in the forward-view videos are different from location to location. For instance, in Trip 29431930, the barrier type of the work zone (f_{Br}) was drum (1); the area type (f_{AT}) was rural (1); the lateral clearance (f_{LAT}) was 6 ft; and the event was at the daylight (0) condition. The QDR of this trip was 1466 vphpl and 1692 vphpl when converted to PBC. The estimated capacity range was from 1541 to 1865 vphpl, with the average capacity being 1668 vphpl.

TABLE 2. LANE CLOSURE 2-1 CAPACITY ESTIMATION FROM HCM

Configuration	Trip ID	LOS	$LCSI$	f_{Br}	f_{AT}	f_{LAT}	f_{DN}	QDR	PBC
LC2-1	29431930	A2	2	1	1	6	0	1466	1693
LC2-1	41956565	A2	2	0	1	1	0	1615	1865
LC2-1	41956948	A2	2	1	1	3	0	1439	1662
LC2-1	61217623	A2	2	1	1	3	0	1439	1662
LC2-1	113613089	C	2	1	1	0	1	1353	1562
LC2-1	113615004	D	2	1	1	0	0	1412	1630
LC2-1	113615012	C	2	1	1	0	0	1412	1630
LC2-1	116154564	B	2	0	1	0	0	1606	1855
LC2-1	116156982	C	2	1	1	3	0	1439	1662
LC2-1	116157653	C	2	0	1	0	0	1606	1855
LC2-1	116158320	B	2	1	1	1	0	1421	1641
LC2-1	131785455	D	2	1	1	3	1	1380	1594
LC2-1	132362892	B	2	1	1	-2	1	1335	1542
LC2-1	133753420	B	2	1	1	0	0	1412	1630
LC2-1	135449627	B	2	1	1	0	0	1412	1630
LC2-1	136380221	C	1.5	1	1	1.5	0	1503	1735
LC2-1	136418655	B	2	1	1	3	0	1439	1662
LC2-1	138351822	A2	2	1	1	3	1	1380	1594
LC2-1	142007555	C	2	1	1	3	0	1439	1662
LC2-1	142050014	A2	2	1	1	3	1	1380	1594

5.1.2 Shoulder Closure

Similarly, the speed-density relationships of shoulder closure 2-2 and 3-3 were also performed, as shown in Figures 9 to 12. For shoulder closure 2-2, the sample size is 24 trips. As presented in Figure 9, the regression model of NDS data indicates the free flow speed of the two-to-two shoulder closure work zone is 74 mph. The jam density is 192 vpmpl. Although the regression model does not fit the data very well with an R^2 of 0.4625, the linear relationship can still be seen. The speed-flow estimation in Figure 10 reveals that the capacity of two-to-two shoulder closure is approximately 3500 vphpl. The capacity of every two-to-two shoulder closure location was also estimated by HCM, as presented in Table 3.

The range of HCM estimation was from 1829 to 2153 vphpl based on different details of work zone configurations. The average capacity of 24 locations was 1991 vphpl.

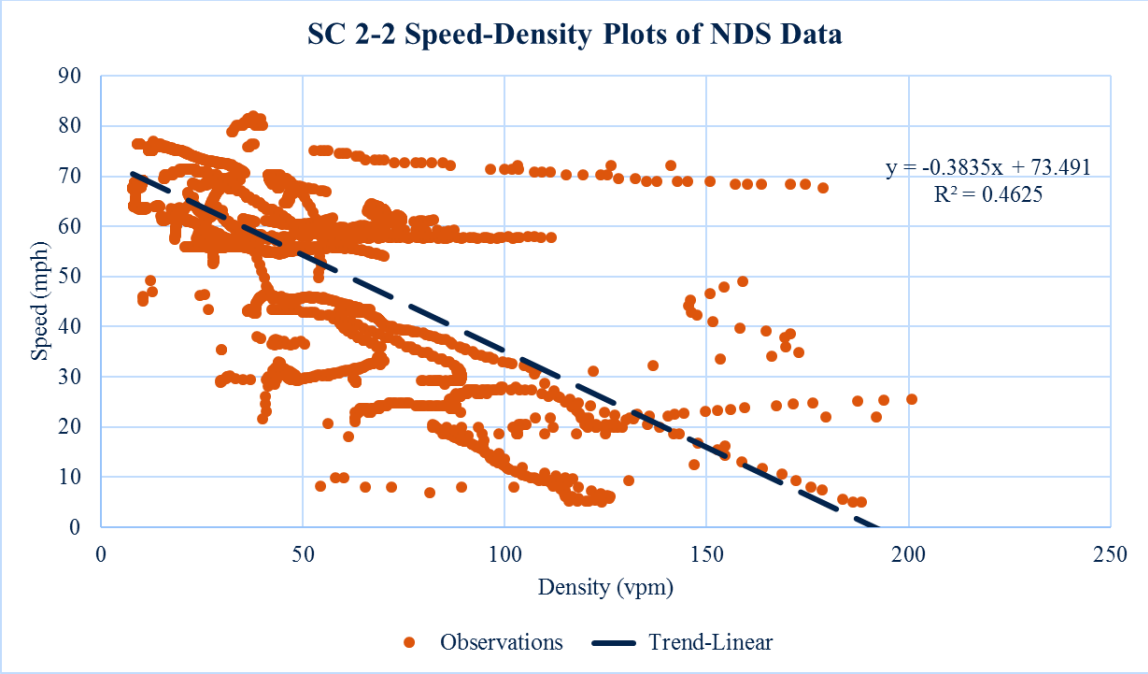

FIGURE 9. SHOULDER CLOSURE 2-2 SPEED-DENSITY PLOTS

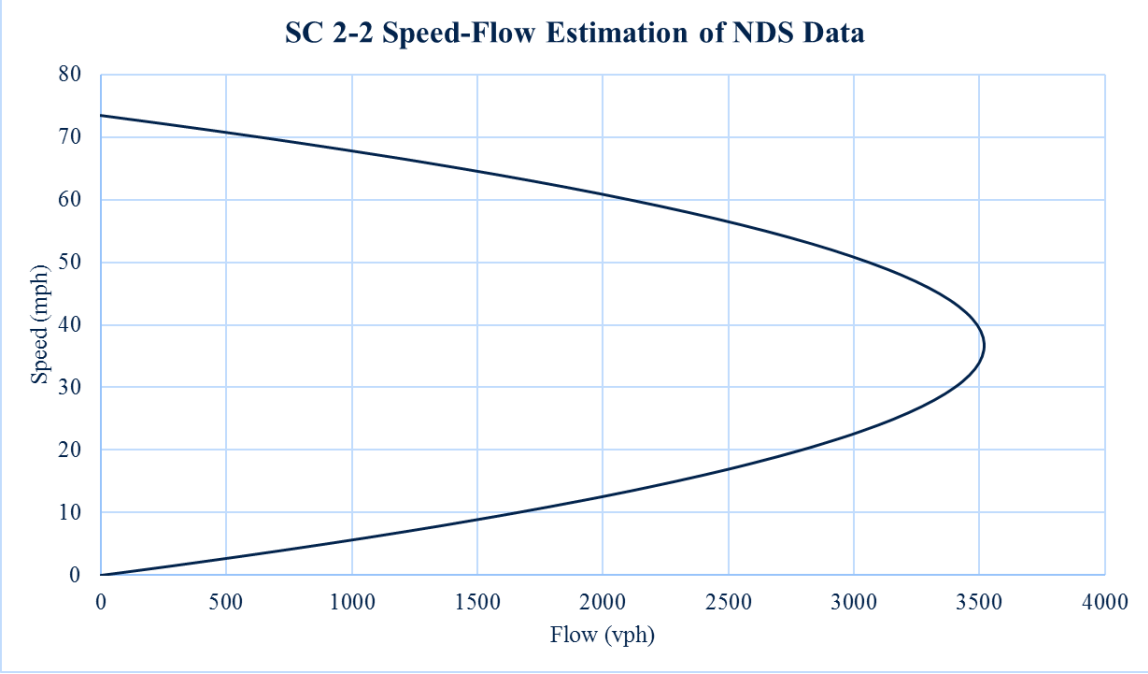

FIGURE 10. SHOULDER CLOSURE 2-2 SPEED-FLOW ESTIMATION

TABLE 3. SHOULDER CLOSURE 2-2 CAPACITY ESTIMATION FROM HCM

Configuration	Trip ID	LOS	$LCSI$	f_{Br}	f_{AT}	f_{LAT}	f_{DN}	QDR	PBC
SC2-2	29431332	B	0.5	0	1	3	0	1864	2152
SC2-2	29866683	B	0.5	0	1	1	0	1846	2132
SC2-2	31297536	D	0.5	0	1	0	0	1837	2121
SC2-2	33564261	A2	0.5	1	1	6	1	1638	1891
SC2-2	41956494	A2	0.5	1	1	10	0	1733	2001
SC2-2	41956909	B	0.5	1	1	6	0	1697	1960
SC2-2	113613588	A2	0.5	0	1	0	1	1778	2053
SC2-2	115730201	C	0.5	1	1	6	0	1697	1960
SC2-2	116156464	A2	0.5	0	1	0	0	1837	2121
SC2-2	116156671	B	0.5	1	1	3	0	1670	1928
SC2-2	116157646	A2	0.5	1	1	3	0	1670	1928
SC2-2	116157964	B	0.5	1	1	6	0	1697	1960
SC2-2	132360678	B	0.5	1	1	10	0	1733	2001
SC2-2	132523892	A2	0.5	1	1	3	0	1670	1928
SC2-2	134032900	D	0.5	0	1	0	0	1837	2121
SC2-2	134049268	B	0.5	1	1	6	0	1697	1960
SC2-2	135126591	B	0.5	1	1	0	1	1584	1829
SC2-2	142012222	A2	0.5	1	1	12	0	1751	2022
SC2-2	142029852	E	0.5	1	1	6	1	1638	1891
SC2-2	142050027	B	0.5	1	1	1	1	1593	1839
SC2-2	142053584	B	0.5	1	1	0	0	1643	1897
SC2-2	151087733	B	0.5	1	1	6	0	1697	1960
SC2-2	151088529	B	0.5	1	1	10	0	1733	2001
SC2-2	151090633	B	0.5	0	1	1	0	1846	2132

In shoulder closure 3-3, there are 32 trips in total. As presented in Figures 11 and 12, the free flow speed predicted in the linear regression model from NDS data is 72 mph and the jam density is 200 vpmpl. The R^2 of the NDS regression model is 0.3849, but the linear relationship between speed and density is quite obvious. The capacity predicted based on Greenshield's model is yielded to 3600 vphpl in the three-to-three shoulder closure work zone. This number is much higher when compared with Table 4, the capacity estimation from HCM. In Table 4, the estimation is from 1921 to 2183 vphpl with an average capacity of 2070 vphpl.

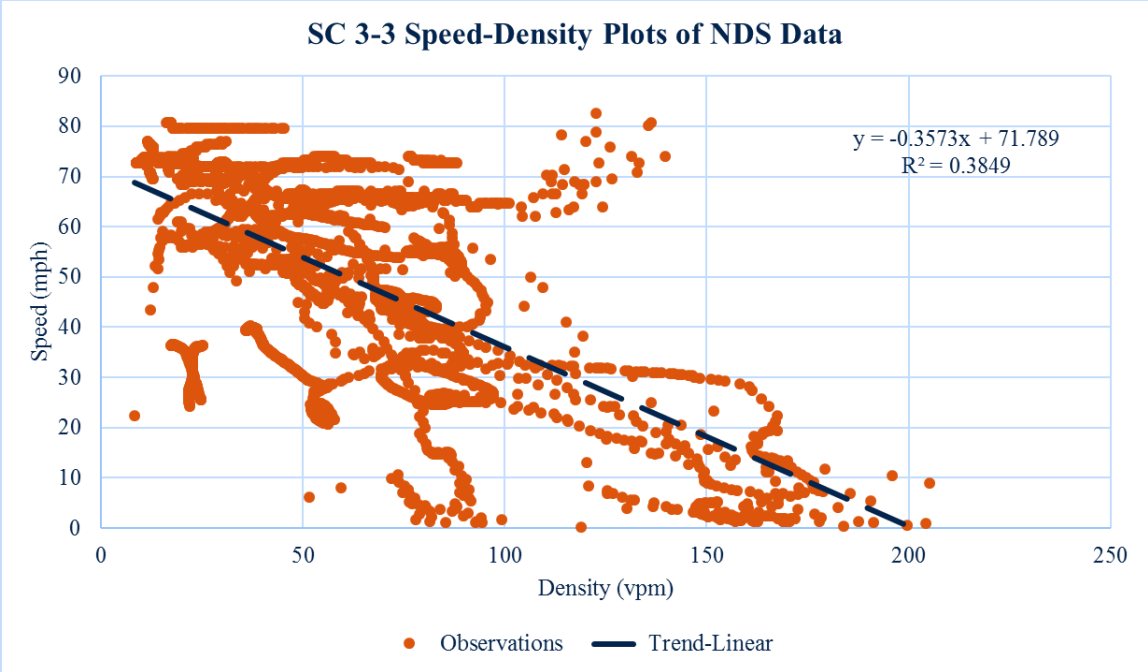

FIGURE 11. SHOULDER CLOSURE 3-3 SPEED-DENSITY PLOTS

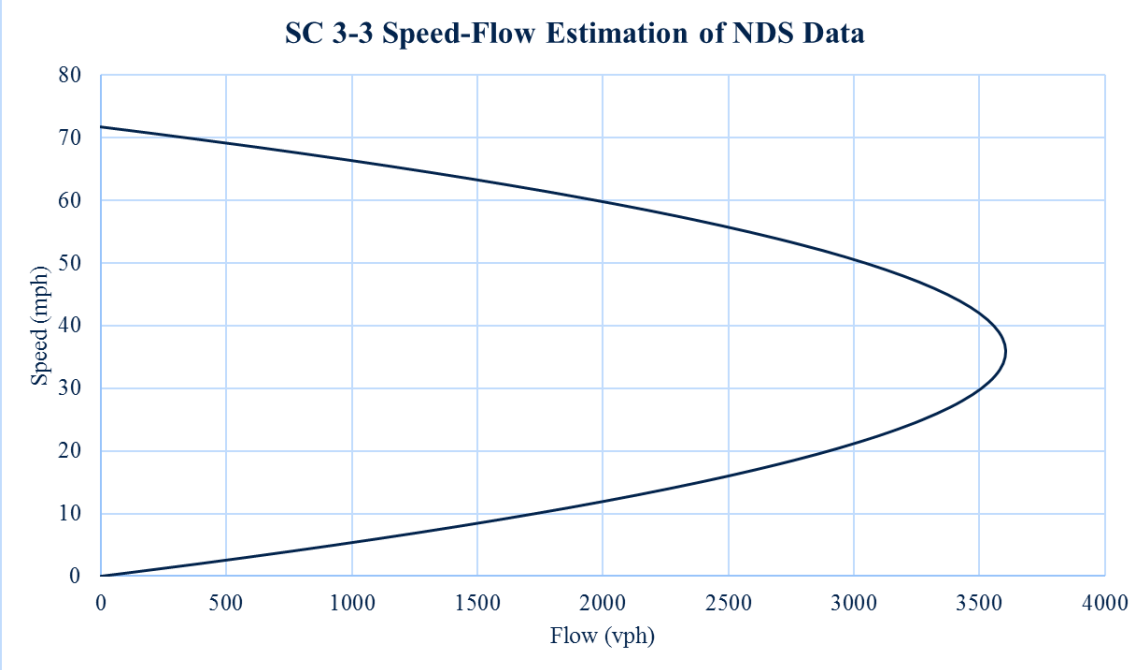

FIGURE 12. SHOULDER CLOSURE 3-3 SPEED-FLOW ESTIMATION

TABLE 4. SHOULDER CLOSURE 3-3 CAPACITY ESTIMATION FROM HCM

Configuration	Trip ID	LOS	$LCSI$	f_{Br}	f_{AT}	f_{LAT}	f_{DN}	QDR	PBC
SC3-3	10858444	C	0.33	0	1	3	0	1890	2183
SC3-3	15108994	B	0.33	0	1	0	0	1863	2151
SC3-3	22303764	D	0.33	0	1	0	0	1863	2151
SC3-3	29714439	A2	0.33	1	1	3	0	1696	1959
SC3-3	29751594	B	0.33	0	1	3	0	1890	2183
SC3-3	29866807	A1	0.33	1	1	6	1	1664	1922
SC3-3	33565881	A2	0.33	1	1	3	0	1696	1959
SC3-3	33566037	A2	0.33	0	1	1	0	1872	2162
SC3-3	35258010	B	0.33	0	1	0	1	1804	2083
SC3-3	36842978	D	0.33	0	1	3	1	1831	2115
SC3-3	98562063	A2	0.33	0	1	1	0	1872	2162
SC3-3	113612691	A2	0.33	1	1	6	1	1664	1922
SC3-3	113614573	B	0.33	1	1	10	1	1700	1963
SC3-3	116153037	C	0.33	1	1	6	0	1723	1990
SC3-3	116155665	B	0.33	0	1	0	0	1863	2151
SC3-3	116156933	B	0.33	0	1	1	0	1872	2162
SC3-3	116158384	B	0.33	1	1	6	1	1664	1922
SC3-3	132362030	C	0.33	1	1	3	0	1696	1959
SC3-3	132370221	C	0.33	1	1	3	0	1696	1959
SC3-3	132699377	B	0.33	0	1	1	0	1872	2162
SC3-3	132699457	C	0.33	0	1	0	0	1863	2151
SC3-3	134041017	C	0.33	0	1	3	0	1890	2183
SC3-3	135187907	A2	0.33	0	1	0	0	1863	2151
SC3-3	135187961	C	0.33	1	1	6	0	1723	1990
SC3-3	135946649	D	0.33	0	1	1	0	1872	2162
SC3-3	138265878	B	0.33	0	1	1	0	1872	2162
SC3-3	138290345	D	0.33	1	1	6	0	1723	1990
SC3-3	138359067	B	0.33	1	1	6	0	1723	1990
SC3-3	138359145	A2	0.33	0	1	0	0	1863	2151
SC3-3	138361411	B	0.33	0	1	1	0	1872	2162
SC3-3	142053320	B	0.33	1	1	3	0	1696	1959
SC3-3	151089332	B	0.33	1	1	3	0	1696	1959

5.1.3 Discussion of Traffic Flow Modeling Results

Three graphs of speed versus density data of lane closure 2-1, shoulder closure 2-2 and 3-3 work zone, and speed versus flow predicted by Greenshield's model were discussed. The capacity estimated by HCM work zone capacity method based on the details of all work zone configurations can be found in Appendix B. Although the R^2 of the regression models is below 0.6, it appears as a solid linear

relationship between speed and density. In addition, the NDS data contain the kinematics of participant vehicle and the front vehicle, which can be treated as a small moving segment. This is similar to the connected vehicle environment, which is one of the reasons of overestimated capacities that can be achieved by connected vehicles. Thus, the NDS data has the potential to be applied to connected vehicle studies. It should also be mentioned that the free flow speeds predicted from NDS regression models are 62 mph for two-to-one lane closure, 73 mph for two-to-two shoulder closure, and 72 mph for three-to-three shoulder closure. This information can be used to improve or calibrate the planning and simulation tools. For instance, the free flow speed, average speed, minimum speed, distance traveled during speed change cycle, average speed in queue, etc. from QUEWZ, which were based on outdated field data and methodology (*21*), can all be modified through complete work zone NDS trips with enough sample size.

5.2 Headway Distribution

Headway distribution analysis includes the time and space headway distributions under three selected work zone configurations. It should be noted that an average vehicle length of 25 ft (*45*) was added to space headway; further, the time headway also included the corresponding time needed for 25 ft.

5.2.1 Time Headway

Table 5 summarizes the descriptive results of time headway distribution in the ten work zone configurations, including maximum, average, high-frequency range, minimum, and standard deviation. For example, in lane closure 2-1, the maximum time headway among the 20 trips is 19.43 s; the average time headway is 1.96 s; most of the drivers selected their time headway from 0.97 to 1.47 s; and the minimum time headway presented is 0.47 s.

TABLE 5. TIME HEADWAY DESCRIPTIVE STATISTICS

Work Zone Configurations		Time Headway (s)					Sample Size
		Maximum	Average	High Frequency	Minimum	Standard Deviation	
Lane Closure	**2-1**	**19.43**	**1.96**	**(0.97, 1.47)**	**0.47**	**1.12**	**20**
	3-2	30.63	2.98	(1.30, 1.80)	0.8	2.72	6
	3-1	3.96	3.67	(3.70, 4.20)	3.2	0.23	1
	4-3	1.37	0.88	(0.59, 1.09)	0.59	0.17	1
	4-2	2.61	2.47	(2.13, 2.63)	2.13	0.15	1
Shoulder Closure	1-1	3.69	1.98	(1.27, 1.77)	0.77	0.8	5
	2-2	**7.96**	**2.13**	**(0.80, 1.3)**	**0.3**	**1.39**	**24**
	3-3	**36.26**	**2.1**	**(0.83, 1.33)**	**0.33**	**2.2**	**32**
	4-4	37.31	2.67	(2.99, 3.49)	0.49	2.9	11

	5-5	3.32	2.65	(2.08, 2.58)	2.08	0.41	1

The time headway distributions from LOS A to D&E are illustrated in Figure 13. Boxplots were utilized to detect potential outliers, which were filtered if they were more than the upper limit or less than the lower limit of each LOS. The average time headways from LOS A to E&F are 2.52, 1.95, 2.05, and 2.55 s, respectively. From the boxplot, the range of the upper quartile (75%) and lower quartile (25%) in average time headway have the tendency to decrease as LOS decreases. This boxplot can also help to determine the work zone capacity. For example, if 2.05 s (average time headway of LOS C) is the capacity headway, the work zone capacity should equal 3600 s divided by 2.05 s, which is 1756 vphpl.

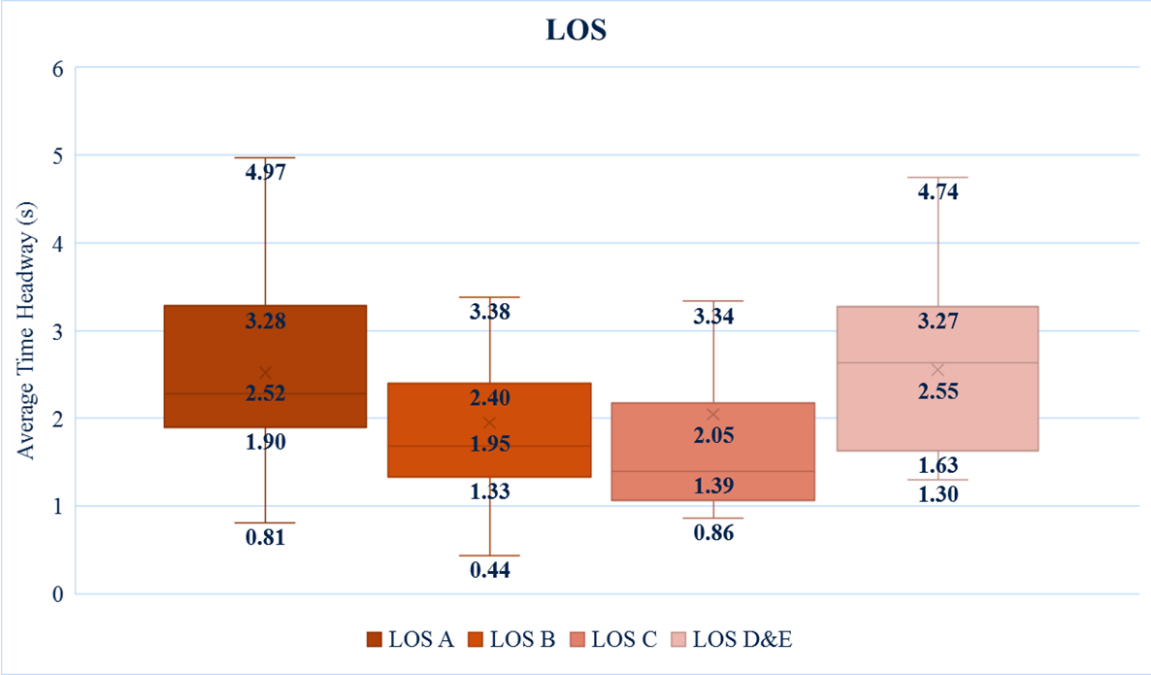

FIGURE 13. TIME HEADWAY DISTRIBUTION AT DIFFERENT LOS

5.2.2 Space Headway

Table 6 lists the descriptive statistics of space headway distribution in the ten work zone configurations. The configurations with enough traversals are emphasized in the table. For example, in lane closure 2-1, the maximum space headway among the 20 trips is 506 ft; the average time headway is 130 ft; the space headway of most drivers ranges from 70 to 110 ft; and the minimum space headway presented is 30 ft.

TABLE 6. SPACE HEADWAY DESCRIPTIVE STATISTICS

Work Zone Configurations		Space Headway (ft)					Sample Size
		Maximum	Average	High Frequency	Minimum	Standard Deviation	
Lane Closure	**2-1**	**506**	**130**	**(70, 110)**	**30**	**90**	**20**
	3-2	618	204	(30, 70)	30	168	6
	3-1	258	234	(214, 254)	174	26	1
	4-3	104	58	(43, 83)	43	11	1
	4-2	225	216	(187, 227)	187	12	1
Shoulder Closure	1-1	266	122	(58, 98)	58	57	5
	2-2	**676**	**175**	**(66, 106)**	**26**	**145**	**24**
	3-3	**628**	**134**	**(66, 106)**	**26**	**94**	**32**
	4-4	465	143	(31, 71)	31	94	11
	5-5	282	226	(175, 215)	175	34.16	1

Figure 14 presents the space headway distributions from LOS A to D&E. Similarly, the potential outliers were filtered by boxplot if they were more than the upper limit or less than the lower limit of each LOS. The average space headways from LOS A to E&F are 213, 140, 98, and 86 ft, respectively. It is obvious that the space headway is decreasing as LOS drops. This boxplot can help to determine the work zone jam density. For example, the average space headway at LOS D&E being 86 ft, and the work zone jam density should equal 5280 ft divided by 86 ft, which is 62 vpmpl. With a limited sample size of LOS D and E and without trips of LOS F, the jam density calculated here might be underestimated.

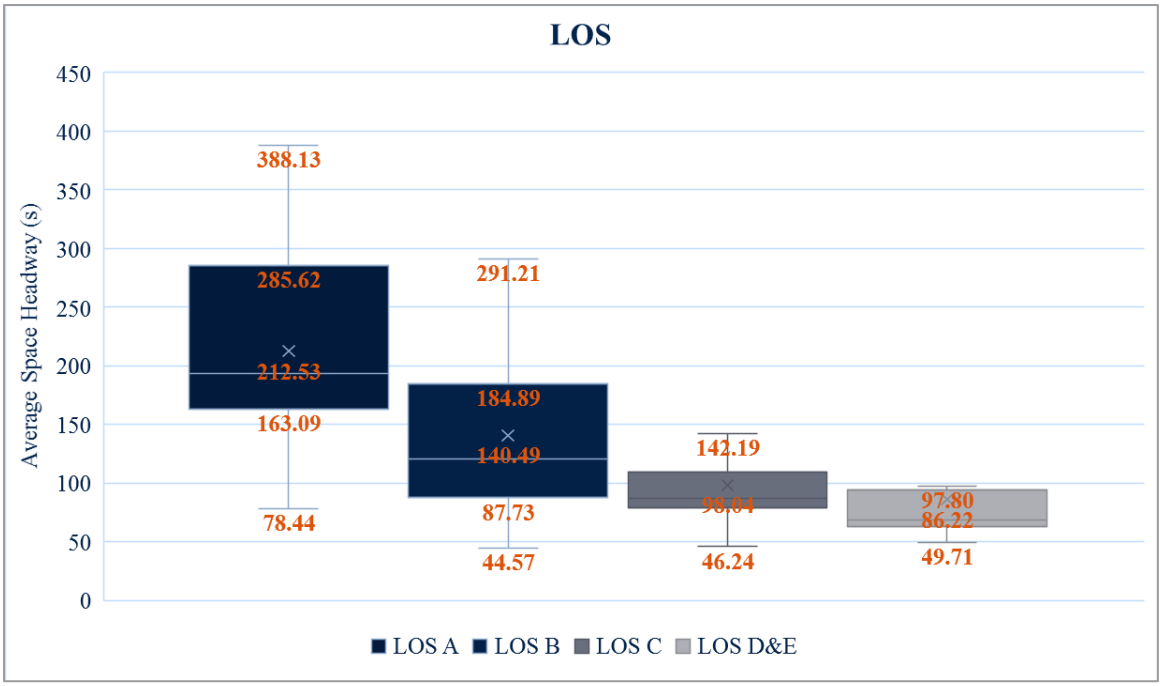

FIGURE 14. SPACE HEADWAY DISTRIBUTION AT DIFFERENT LOS

5.2.3 Driver Risk Perception

Driver risk perception is an indicator of whether the driver is aggressive or timid. As presented in Figure 15, more than 70% of drivers in the sample have a risk perception score greater than 148, which indicates these participants have greater risk perceptions and tend to be cautious and obedient to traffic rules. In total, there were 38 female drivers and 42 male drivers.

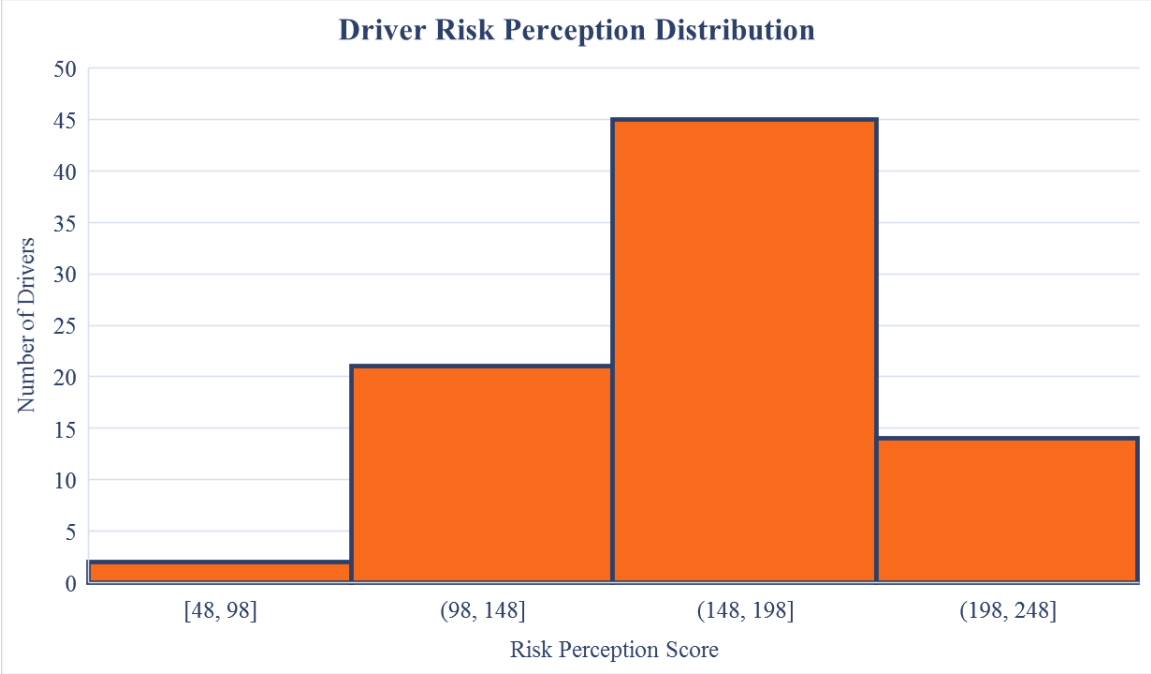

FIGURE 15. DRIVER RISK PERCEPTION DISTRIBUTION

Figure 16 indicates that male drivers are likely to maintain a slightly longer time headway. The average time headway of male drivers (2.6 s) is greater than that for female drivers (2.0 s), but the headway convergence of female drivers reveals that the female drivers' headway selections are consistent.

In addition, female drivers seem to be more timid because their risk scores are higher, as shown in Figure 17. However, there is no significant difference between male and female drivers toward the risk perception scores.

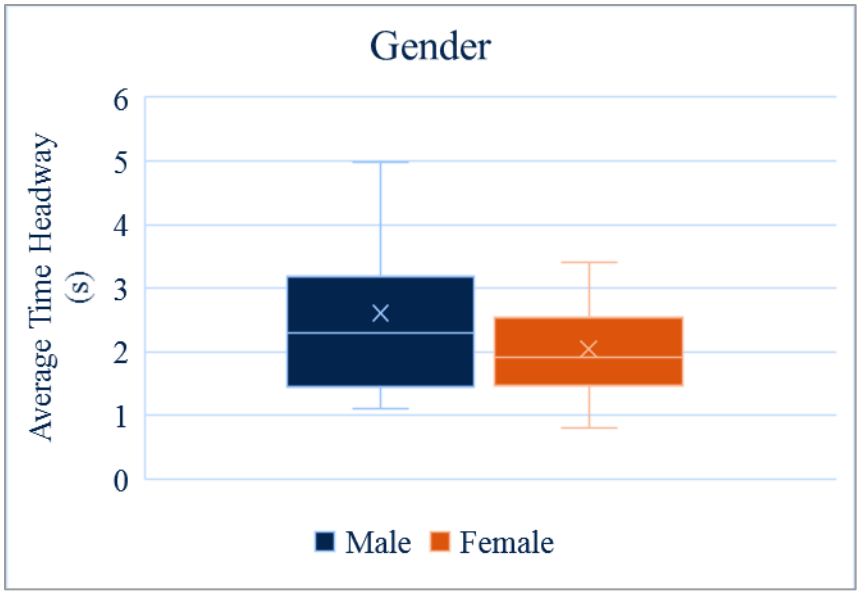

FIGURE 16. AVERAGE TIME HEADWAY BASED ON GENDER

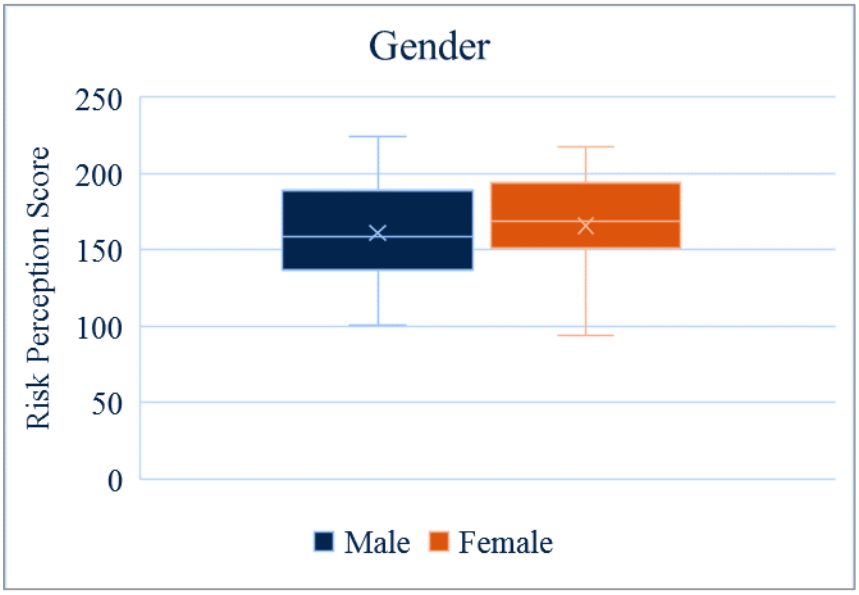

FIGURE 17. RISK PERCEPTION SCORE BASED ON GENDER

Figure 18 conveys the average time headway distribution based on the age group. The young drivers less than 24 years of age appear to maintain 2.1 s time headway. The middle-aged drivers from 24 to 60 select their time headway as 2.4 s. The average time headway of senior drivers is the longest at 2.6 s.

As for the risk perception score based on the age group, a similar trend can be found in Figure 19. The risk perception of teen drivers younger than 24 was found to be the lowest, which indicates that teen drivers tend to take more risks when driving.

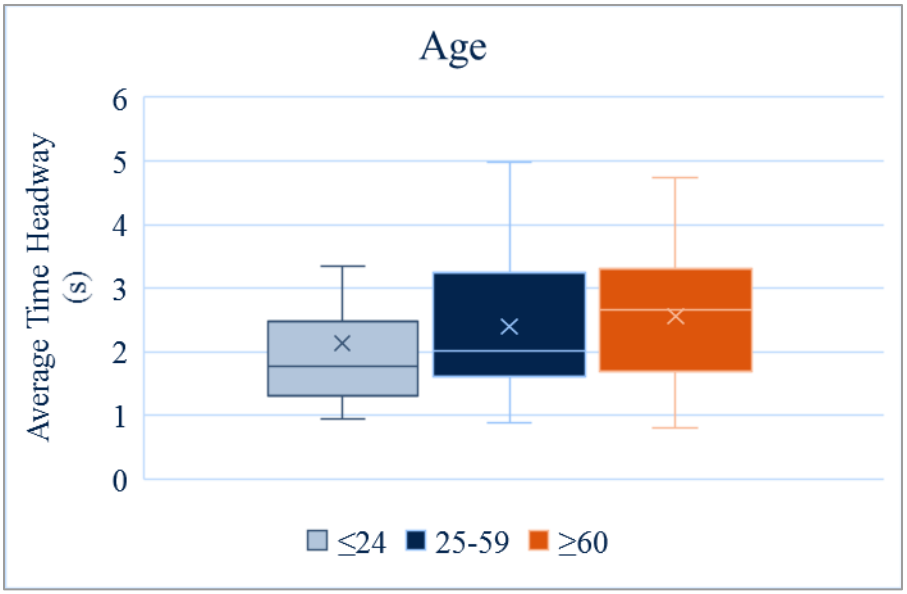

FIGURE 18. AVERAGE TIME HEADWAY BASED ON AGE

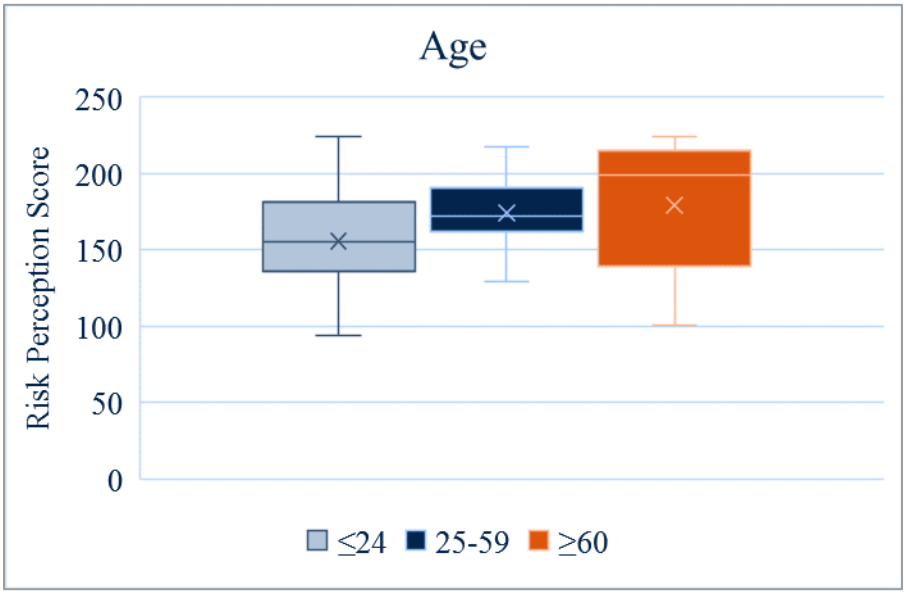

FIGURE 19. RISK PERCEPTION SCORE BASED ON AGE

5.2.4 Discussions of Headway Distribution Results

Time and space headway and their relations with driver characteristics of ten work zone configurations were analyzed. The relationship between headway and LOS was identified. More specific headway distributions of lane closure 2-1 and shoulder closure 2-2 and 3-3 can be found in Appendix B. It is reasonable that the space headway decreases as LOS drops because the more congested the closer between vehicles. In addition, it was found that 85% of the drivers selected their time headway from 0.8 to 2.8 s and 50 to 175 ft in space headway.

Table 7 summarizes the details of headway distribution (time and space headways) and driver characteristics (gender, age group, and driver risk perceptions). It includes the high-frequency ranges and average values of risk perception scores, time and space headways from drivers by age group and gender. It is interesting that female drivers from all age groups have a constant risk perception of approximately 150 to 210. While male drivers from different age groups distribute differently. The risk perception score of male drivers under the age of24 ranges from 114 to 164, but senior male drivers have a range from 165 to 215. The risk score range of middle age (25-59) male drivers is also in the middle compared with young (≤24) and senior (≥60) drivers, being from 129 to 179. The risk perceptions of female drivers from all age groups are higher than those of male drivers. However, their average time headways are typically smaller than those of male drivers. As shown in Table 7, the average time headway for young female drivers is 1.84, while it is 2.27 for young male drivers.

The headway distributions from different drivers will be useful to estimate the work zone capacity at the planning level. Because driving behaviors from different genders and age groups are not the same, this will have an influence on the work zone capacity. Thus, there is also potential to add a driver population factor in estimating work zone capacity based on local population conditions.

TABLE 7. HEADWAY DISTRIBUTION AND DRIVER CHARACTERISTICS

Gender	Characteristic		Age Group		
			≤24	25-59	≥60
Female Driver	Sample Size		22	13	3
	Risk	High Frequency	(148, 198)	(149, 199)	(158, 208)
		Average	160	183	191
	Time Headway (s)	High Frequency	(0.86, 1.36)	(1.39, 1.89)	(0.81, 3.28)
		Average	1.84	2.35	1.97
	Space Headway (ft)	High Frequency	(90, 130)	(46, 86)	(78, 222)
		Average	119	169	154
Male Driver	Sample Size		24	10	8
	Risk	High Frequency	(114, 164)	(129, 179)	(165, 215)
		Average	153	165	175
	Time Headway (s)	High Frequency	(1.44, 1.94)	(0.88, 1.38)	(1.19, 1.69)
		Average	2.27	2.43	2.78
	Space Headway (ft)	High Frequency	(85, 125)	(98, 138)	(79, 295)
		Average	131	155	196

6.0 CONCLUSION

This project is a one-year proof-of-concept project to ascertain if the existing NDS work zone database can be reused to develop new (or update existing) capacity and traffic flow models for work zones. It utilized a complimentary NDS data set to evaluate the traffic flows in three different freeway work zone configurations. The study found that NDS data provide a unique opportunity to study car-following models for different driver types in different work zone configurations. Due to the limitations of the complimentary NDS data (small sample size and short trip length), this study is unable to develop robust recommendations for updating current work zone capacity analysis methods. Some preliminary findings are as follows:

- The NDS data can be used to develop the relationship between speed and flow. It can be used to compare with the HCM method. In this study, it was found that the capacities estimated from HCM are typically smaller than those from NDS speed-flow regression models. In addition, a linear relationship appears between speed and density.
- The NDS data show the potential to improve and calibrate the planning and simulation tools. For example, the free flow speeds estimated from NDS speed-density regression models for LC 2-1, SC 2-2, and SC 3-3 are 62, 73, and 72 mph, respectively. With more complete work zone NDS trips, more parameters such as distance traveled during speed change cycle and average speed in queue can be established for the planning software QUEWZ.
- The NDS data can be used to develop car-following models for different congestion levels. It was found that the headway decreases as LOS drops. In addition, it was found that 85% of the drivers selected their time headway from 0.8 to 2.8 s and 50 to 175 ft in space headway.
- The NDS data can be used to study the headway selection by driver types. For instance, this study suggested that:
    - Male drivers are likely to maintain a slightly longer time headway. The average time headway of male drivers (2.6 s) is greater than female drivers (2.0 s), but the headway convergence of female drivers reveals that the female drivers' headway selections are more consistent.
    - Senior drivers were found to choose longer time headway when passing a work zone. Young drivers age less than 24 appear to maintain 2.1 s time headway. The middle-aged drivers from 25 to 59 select their time headway as 2.4 s. The average time headway of senior drivers is the longest of 2.6 s.
    - Based on the risk perception, female drivers seem to be more timid because their risk scores are higher than those of male drivers. The risk perceptions of teen drivers younger than 24 were found to be the lowest among three age groups, which indicates that teens tend to take more risks when driving.

7.0 RECOMMENDATIONS

In the next step, the focus should be on five more specific work zone configurations on the freeway, including lane closure 3-2, 3-1, 2-1 and shoulder closure 3-3, 2-2. Trips traversing the entire work zone area (2,000 ft upstream, advanced warning area, transition area, activity area, termination area, 2,000 ft downstream) and locations with at least 50 trips should be requested. Moreover, the number of LOS E and F trips should be greater than 10. The speed, acceleration rate, brake pedal usage or position, gas pedal usage or position should be requested in the time-series data. The radar data, forward-view, rear-view videos, and driver risk perceptions should also be requested.

The recommended further tasks are summarized below:

- Identify the speed-flow-density relationship for lane closure 3-2, 3-1, 2-1, and shoulder closure 3-3, 2-2. The capacities of different work zone configurations will be estimated.
- Explore how driver types (i.e., gender, age group, risk perception, etc.) and car-following behaviors (e.g., space and time headway selection) impact on work zone capacity.
- Develop car-following models to improve work zone capacity methods and other work zone planning and simulation tools. Verify and calibrate the work zone capacity method defined by HCM.

8.0 REFERENCE LIST

1. FHWA Work Zone Facts and Statistics. Work Zone Management Program. FHWA. U.S. Department of Transportation. https://ops.fhwa.dot.gov/wz/resources/facts_stats.htm. Accessed Mar. 5, 2019.
2. Yeom, C., N.M. Rouphail, and W. Rasdorf. Simulation Guidance for Freeway Lane Closure Capacity Calibration. Transportation Research Record: Journal of the Transportation Research Board, 2015. 2553: 82-89.
3. Weng, J. and Q. Meng. Incorporating Work Zone Configuration Factors into Speed-Flow and Capacity Models. Journal of Advanced Transportation, 2015. 49(3): 371–384.
4. Weng, J. and Q. Meng. Decision Tree-Based Model for Estimation of Work Zone Capacity. Transportation Research Record: Journal of the Transportation Research Board, 2011. 2257: 40-50.
5. Highway Capacity Manual 6th Edition: A Guide for Multimodal Mobility Analysis. Transportation Research Board., Washington, D.C., 2016.
6. Weng, J. and Q. Meng. Ensemble Tree Approach to Estimating Work Zone Capacity. Transportation Research Record: Journal of the Transportation Research Board, 2012. 2286: 56–67.
7. Heaslip, K., A. Kondyli, D. Arguea, L. Elefteriadou, and F. Sullivan. Estimation of Freeway Work Zone Capacity through Simulation and Field Data. Transportation Research Record: Journal of the Transportation Research Board, 2009. 2130: 16–24.
8. Kan, X., H. Ramezani, and R. F. Benekohal. Calibration of VISSIM for Freeway Work Zones with Time Varying Capacity. Presented at 93rd Annual Meeting of the Transportation Research Board, Washington, D.C., 2014.
9. Chatterjee, I., P. Edara, S. Menneni, and C. Sun. Replication of Work Zone Capacity Values in a Simulation Model. Transportation Research Record: Journal of the Transportation Research Board, 2009. 2130: 138–148.
10. Heaslip, K., M. Jain, and L. Elefteriadou. Estimation of Arterial Work Zone Capacity using Simulation. Transportation Letters, 2011. 3(2): 123–134.
11. Sarasua, W. A., W. J. Davis, M. A. Chowdhury, and J. H. Ogle. Estimating Interstate Highway Capacity for Short-Term Work Zone Lane Closures: Development of Methodology. Transportation Research Record: Journal of the Transportation Research Board, 2006. 1948: 45–57.
12. Dingus, T. A., J. M. Hankey, J. F. Antin, S. E. Lee, L. Eichelberger, K. E. Stulce, D. McGraw, M. Perez, and L. Stowe. Naturalistic Driving Study: Technical Coordination and Quality Control. SHRP 2 Report S2-S06-RW-1. FHWA, U.S. Department of Transportation, 2015.
13. Evaluation of Work Zone Safety Using the SHRP 2 Naturalistic Driving Study Data. Shauna Hallmark, Omar Smadi, and Anuj Sharma. Center for Transportation Research and Education at Iowa State University's Institute for Transportation, Ames. http://shrp2.transportation.org/Documents/03-SHRP2%20IAP%20Round%204-MNWork%20Zones.pdf. Accessed Mar. 5, 2019.

14. A Multidisciplinary Approach to Investigate Work Zone Safety using SHRP 2 Safety Data. Praveen Edara and Omar Smardi. University of Missouri, Columbia. https://mtc.intrans.iastate.edu/research/in-progress/a-multidisciplinary-approach-to-investigate-work-zone-safety-using-shrp-2-safety-data/. Accessed Mar. 5, 2019.
15. Analysis of SHRP2 Data to Understand Normal and Abnormal Driving Behavior in Work Zones: Phase II. Selpi Selpi, Jordanka Kovaceva, and Robert Thomson. University of Michigan Transportation Research Institute, Ann Arbor. https://www.chalmers.se/en/projects/Pages/Analysis-of-SHRP2-Data-to-Understand-Normal-and-Abnormal-Driving.aspx. Accessed Mar. 5, 2019.
16. Dowling, R., A. Skabardonis, and V. Alexiadis. Traffic Analysis Toolbox Volume III: Guidelines for Applying Traffic Microsimulation Modeling Software. Publication FHWA-HRT-04-040. FHWA, U.S. Department of Transportation, 2004.
17. Zhang, L., D. Morallos, K. Jeannotte, and J. Strasser. Traffic Analysis Toolbox Volume XII: Work Zone Traffic Analysis–Applications and Decision Framework. Publication FHWA-HOP-12-009. FHWA, U.S. Department of Transportation, 2012.
18. Alexiadis, V., K. Jeannotte, and A. Chandra. Traffic Analysis Toolbox Volume I: Traffic Analysis Tools Primer. Publication FHWA-HRT-04-038. FHWA, U.S. Department of Transportation, 2004.
19. Benekohal, R. F., A. Z. Kaja-Mohideen, and M. V. Chitturi. Evaluation of Construction Work Zone Operational Issues: Capacity, Queue, and Delay. Publication ITRC FR 00/01-4. Illinois Transportation Research Center, 2003.
20. Ramezani, H., and R. F. Benekohal. Work Zones as a Series of Bottlenecks. Transportation Research Record: Journal of the Transportation Research Board, 2012. 2272: 67–77.
21. Ishimaru, J., and M. Hallenbeck. QUEWZ Work Zone Software: Literature Search and Methodology Review. WA-RD 888.1. Washington State Department of Transportation, 2019.
22. Trask, L., B. Aghdashi, B. Schroeder, and N. Rouphail. FREEVAL-WZ Users Guide. North Carolina State University, Raleigh, NC. 2015.
23. Mahmassani, H. S., H. Sbayti, and X. Zhou. DYNASMART-P Version 1.0 User's Guide. Maryland Transportation Initiative, College Park, MD. 2004.
24. Adeli, H., and X. Jiang. Neuro-Fuzzy Logic Model for Freeway Work Zone Capacity Estimation. Journal of Transportation Engineering, 2003. 129(5): 484–493.
25. Corder, G. W. and D. I. Foreman. Nonparametric statistics: A step-by-step approach. John Wiley & Sons, Inc., New York, 2014.
26. Non-parametric Methods. R Tutorial: An R Introduction to Statistics. http://www.r-tutor.com/elementary-statistics/non-parametric-methods. Accessed Mar. 5, 2019
27. Lu, C., J. Dong, A. Sharma, T. Huang, and S. Knickerbocker. Predicting Freeway Work Zone Capacity Distribution Based on Logistic Speed-Density Models. Journal of Advanced Transportation, 2018.

28. Karim, A. and H. Adeli. Radial Basis Function Neural Network for Work Zone Capacity and Queue Estimation. Journal of Transportation Engineering, 2003. 129(5): 494-503.
29. Weng, J., and Q. Meng. Estimating Capacity and Traffic Delay in Work Zones: An Overview. Transportation Research Part C: Emerging Technologies, 2013. 35: 34-45.
30. Krammes, R. A. and G. O. Lopez. Updated Capacity Values for Short-Term Freeway Work Zone Lane Closures. Transportation Research Record: Journal of the Transportation Research Board, 1994. 1442: 49–56.
31. T. Kim, D. J. Lovell, M. Hall, and J. Paracha. A New Methodology to Estimate Capacity for Freeway Work Zones. Presented at 80th Annual Meeting of the Transportation Research Board, Washington, D.C., 2000.
32. Al-Kaisy, A., M. Zhou, and F. Hall. New Insights into Freeway Capacity at Work Zones: Empirical Case Study. Transportation Research Record: Journal of the Transportation Research Board, 2000. 1710: 154–160.
33. Al-Kaisy, A. and F. Hall. Guidelines for Estimating Capacity at Freeway Reconstruction Zones. Journal of Transportation Engineering, 2003. 129(5): 572–577.
34. Racha, S., M. Chowdhury, W. Sarasua, and Y. Ma. Analysis of Work Zone Traffic Behavior for Planning Applications. Transportation Planning and Technology, 2008. 31(2): 183–199.
35. Avrenli, K. A., R. Benekohal, and H. Ramezani. Determining Speed-Flow Relationship and Capacity for Freeway Work Zone with No Lane Closure. Presented at 90th Annual Meeting of the Transportation Research Board, Washington, D.C., 2011.
36. Bharadwaj, N., P. Edara, C. Sun, H. Brown, and Y. Chang. Traffic Flow Modeling of Diverse Work Zone Activities. Transportation Research Record: Journal of the Transportation Research Board, 2018. 2676(16): 23-34.
37. Benekohal, R.F., A.Z. Kaja-Mohideen, M. Chitturi. Methodology for Estimating Operating Speed and Capacity in Work Zone. Transportation Research Record: Journal of the Transportation Research Board, 2004. 1833: 103-111.
38. Bharadwaj, N., P. Edara, and C. Sun. Risk Factors in Work Zone Safety Events: A Naturalistic Driving Study Analysis. Transportation Research Record: Journal of the Transportation Research Board, 2019. 0361198118821630.
39. Chang, Y. and P. Edara. Predicting Hazardous Events in Work Zones using Naturalistic Driving Data. Presented at 2017 IEEE 20th International Conference on Intelligent Transportation Systems (ITSC), 2017. IEEE.
40. Abodo, F., R. Rittmuller, B. Sumner, and A. Berthaume. Detecting Work Zones in SHRP 2 NDS Videos Using Deep Learning Based Computer Vision. Presented at 2018 17th IEEE International Conference on Machine Learning and Applications (ICMLA), 2018. IEEE.
41. Liu, Y. A Study on Merging and Diverging Area Design for Urban Underground Expressway. Procedia engineering, 2016. 165: 175-183.
42. Cassidy, M.J. and Rudjanakanoknad J. Increasing the Capacity of an Isolated Merge by Metering its On-Ramp. Transportation Research Part B, 2005. 39: 896–913.

43. Jin, W. A Multi-Commodity Lighthill–Whitham–Richards Model of Lane-Changing Traffic Flow. Transportation Research Part B, 2013. 57: 361–377.
44. Hall, F.L., 1996. Traffic stream characteristics. Traffic Flow Theory. FHWA. 1996.
45. Cascetta, E. Transportation Systems Engineering: Theory and Methods. Springer Science & Business Media, 2013. 49.
46. Introduction to Transportation engineering. Mathew, T. V. and K. K. Rao. Civil Engineering–Transportation Engineering. IIT Bombay, NPTEL ONLINE, http://www. cdeep. iitb. ac. in/nptel/Civil% 20Engineering. Accessed Mar. 5, 2019.
47. Evaluation of Average Effective Vehicle Length in Queue. New England Section ITE Technical Committee. http://neite.org/Documents/Technical/ITE%20Tech%20Comm%20Queue%20Study-Final.pdf. Accessed Mar. 5, 2019.
48. Transportation Research Board of the National Academies of Science. The 2nd Strategic Highway Research Program Naturalistic Driving Study Dataset. Available from the SHRP2 NDS InSight Data Dissemination web site: https://insight.shrp2nds.us. Accessed Mar. 5, 2019.

9.0 APPENDICES

9.1 Appendix A – Acronyms, abbreviations, etc.

NHS	National Highway System
FHWA	Federal Highway Administration
HCM	Highway Capacity Manual
NDS	Naturalistic Driving Study
SHRP2	The Second Strategic Highway Research Program
RID	Roadway Information Database
QDR	Queue Discharge Rate
PBC	Pre-Breakdown Capacity
VTTI	Virginia Tech Transportation Institute
IRB	Institutional Review Boards
LOS	Level of Service
LC	Lane Closure
SC	Shoulder Closure

9.2 Appendix B – Associated websites, data, etc., produced

TABLE 8. ALL TRIPS CAPACITY ESTIMATION FROM HCM

Configuration	Trip ID	LOS	LCSI	F_{br}	F_{at}	F_{lat}	F_{dn}	QDR	PBC
LC2-1	29431930	A2	2	1	1	6	0	1466.00	1692.84
LC2-1	41956565	A2	2	0	1	1	0	1615.00	1864.90
LC2-1	41956948	A2	2	1	1	3	0	1439.00	1661.66
LC2-1	61217623	A2	2	1	1	3	0	1439.00	1661.66
LC2-1	113613089	C	2	1	1	0	1	1353.00	1562.36
LC2-1	113615004	D	2	1	1	0	0	1412.00	1630.48
LC2-1	113615012	C	2	1	1	0	0	1412.00	1630.48
LC2-1	116154564	B	2	0	1	0	0	1606.00	1854.50
LC2-1	116156982	C	2	1	1	3	0	1439.00	1661.66
LC2-1	116157653	C	2	0	1	0	0	1606.00	1854.50
LC2-1	116158320	B	2	1	1	1	0	1421.00	1640.88
LC2-1	131785455	D	2	1	1	3	1	1380.00	1593.53
LC2-1	132362892	B	2	1	1	-2	1	1335.00	1541.57
LC2-1	133753420	B	2	1	1	0	0	1412.00	1630.48
LC2-1	135449627	B	2	1	1	0	0	1412.00	1630.48
LC2-1	136380221	C	1.5	1	1	1.5	0	1502.50	1734.99
LC2-1	136418655	B	2	1	1	3	0	1439.00	1661.66
LC2-1	138351822	A2	2	1	1	3	1	1380.00	1593.53
LC2-1	142007555	C	2	1	1	3	0	1439.00	1661.66
LC2-1	142050014	A2	2	1	1	3	1	1380.00	1593.53
LC3-1	98562841	A2	3	1	1	3	1	1226.00	1415.70
LC3-2	29858067	D	0.75	1	1	6	0	1658.50	1915.13
LC3-2	33564691	A2	0.75	1	1	3	1	1572.50	1815.82
LC3-2	41956916	A2	0.75	1	1	3	1	1572.50	1815.82
LC3-2	115729110	B	0.75	1	1	6	0	1658.50	1915.13
LC3-2	133297582	B	0.75	1	1	3	0	1631.50	1883.95
LC3-2	142011345	A2	0.75	1	1	6	0	1658.50	1915.13
LC4-2	113612612	A1	1	1	1	3	1	1534.00	1771.36
LC4-3	133297580	B	0.44	1	1	3	1	1620.24	1870.95
SC1-1	29714557	B	1	1	1	3	1	1534.00	1771.36
SC1-1	33565846	A2	1	1	1	1	0	1575.00	1818.71
SC1-1	132361153	B	1	0	1	0	0	1760.00	2032.33
SC1-1	151567044	B	1	0	1	0	0	1760.00	2032.33
SC2-2	29431332	B	0.5	0	1	3	0	1864.00	2152.42
SC2-2	29866683	B	0.5	0	1	1	0	1846.00	2131.64
SC2-2	31297536	D	0.5	0	1	0	0	1837.00	2121.25
SC2-2	33564261	A2	0.5	1	1	6	1	1638.00	1891.45
SC2-2	41956494	A2	0.5	1	1	10	0	1733.00	2001.15

Configuration	Trip ID	LOS	LCSI	F_{br}	F_{at}	F_{lat}	F_{dn}	QDR	PBC
SC2-2	41956909	B	0.5	1	1	6	0	1697.00	1959.58
SC2-2	113613588	A2	0.5	0	1	0	1	1778.00	2053.12
SC2-2	115730201	C	0.5	1	1	6	0	1697.00	1959.58
SC2-2	116156464	A2	0.5	0	1	0	0	1837.00	2121.25
SC2-2	116156671	B	0.5	1	1	3	0	1670.00	1928.41
SC2-2	116157646	A2	0.5	1	1	3	0	1670.00	1928.41
SC2-2	116157964	B	0.5	1	1	6	0	1697.00	1959.58
SC2-2	132360678	B	0.5	1	1	10	0	1733.00	2001.15
SC2-2	132523892	A2	0.5	1	1	3	0	1670.00	1928.41
SC2-2	134032900	D	0.5	0	1	0	0	1837.00	2121.25
SC2-2	134049268	B	0.5	1	1	6	0	1697.00	1959.58
SC2-2	135126591	B	0.5	1	1	0	1	1584.00	1829.10
SC2-2	142012222	A2	0.5	1	1	12	0	1751.00	2021.94
SC2-2	142029852	E	0.5	1	1	6	1	1638.00	1891.45
SC2-2	142050027	B	0.5	1	1	1	1	1593.00	1839.49
SC2-2	142053584	B	0.5	1	1	0	0	1643.00	1897.23
SC2-2	151087733	B	0.5	1	1	6	0	1697.00	1959.58
SC2-2	151088529	B	0.5	1	1	10	0	1733.00	2001.15
SC2-2	151090633	B	0.5	0	1	1	0	1846.00	2131.64
SC3-3	10858444	C	0.33	0	1	3	0	1890.18	2182.66
SC3-3	15108994	B	0.33	0	1	0	0	1863.18	2151.48
SC3-3	22303764	D	0.33	0	1	0	0	1863.18	2151.48
SC3-3	29714439	A2	0.33	1	1	3	0	1696.18	1958.64
SC3-3	29751594	B	0.33	0	1	3	0	1890.18	2182.66
SC3-3	29866807	A1	0.33	1	1	6	1	1664.18	1921.69
SC3-3	33565881	A2	0.33	1	1	3	0	1696.18	1958.64
SC3-3	33566037	A2	0.33	0	1	1	0	1872.18	2161.87
SC3-3	35258010	B	0.33	0	1	0	1	1804.18	2083.35
SC3-3	36842978	D	0.33	0	1	3	1	1831.18	2114.53
SC3-3	98562063	A2	0.33	0	1	1	0	1872.18	2161.87
SC3-3	113612691	A2	0.33	1	1	6	1	1664.18	1921.69
SC3-3	113614573	B	0.33	1	1	10	1	1700.18	1963.26
SC3-3	116153037	C	0.33	1	1	6	0	1723.18	1989.82
SC3-3	116155665	B	0.33	0	1	0	0	1863.18	2151.48
SC3-3	116156933	B	0.33	0	1	1	0	1872.18	2161.87
SC3-3	116158384	B	0.33	1	1	6	1	1664.18	1921.69
SC3-3	132362030	C	0.33	1	1	3	0	1696.18	1958.64
SC3-3	132370221	C	0.33	1	1	3	0	1696.18	1958.64
SC3-3	132699377	B	0.33	0	1	1	0	1872.18	2161.87
SC3-3	132699457	C	0.33	0	1	0	0	1863.18	2151.48
SC3-3	134041017	C	0.33	0	1	3	0	1890.18	2182.66

Configuration	Trip ID	LOS	LCSI	F_{br}	F_{at}	F_{lat}	F_{dn}	QDR	PBC
SC3-3	135187907	A2	0.33	0	1	0	0	1863.18	2151.48
SC3-3	135187961	C	0.33	1	1	6	0	1723.18	1989.82
SC3-3	135946649	D	0.33	0	1	1	0	1872.18	2161.87
SC3-3	138265878	B	0.33	0	1	1	0	1872.18	2161.87
SC3-3	138290345	D	0.33	1	1	6	0	1723.18	1989.82
SC3-3	138359067	B	0.33	1	1	6	0	1723.18	1989.82
SC3-3	138359145	A2	0.33	0	1	0	0	1863.18	2151.48
SC3-3	138361411	B	0.33	0	1	1	0	1872.18	2161.87
SC3-3	142053320	B	0.33	1	1	3	0	1696.18	1958.64
SC3-3	151089332	B	0.33	1	1	3	0	1696.18	1958.64
SC4-4	10528092	D	0.25	1	1	10	0	1771.50	2045.61
SC4-4	15363638	C	0.25	1	1	3	0	1708.50	1972.86
SC4-4	60631677	B	0.25	1	1	6	0	1735.50	2004.04
SC4-4	64553434	D	0.25	1	1	0	1	1622.50	1873.56
SC4-4	113613853	B	0.25	0	1	0	0	1875.50	2165.70
SC4-4	116155408	A2	0.25	1	1	10	0	1771.50	2045.61
SC4-4	116155583	D	0.25	1	1	0	0	1681.50	1941.69
SC4-4	134035123	C	0.25	1	1	6	0	1735.50	2004.04
SC4-4	134938558	B	0.25	1	1	6	0	1735.50	2004.04
SC4-4	142005152	B	0.25	1	1	10	0	1771.50	2045.61
SC5-5	116152721	B	0.2	0	1	0	0	1883.20	2174.60

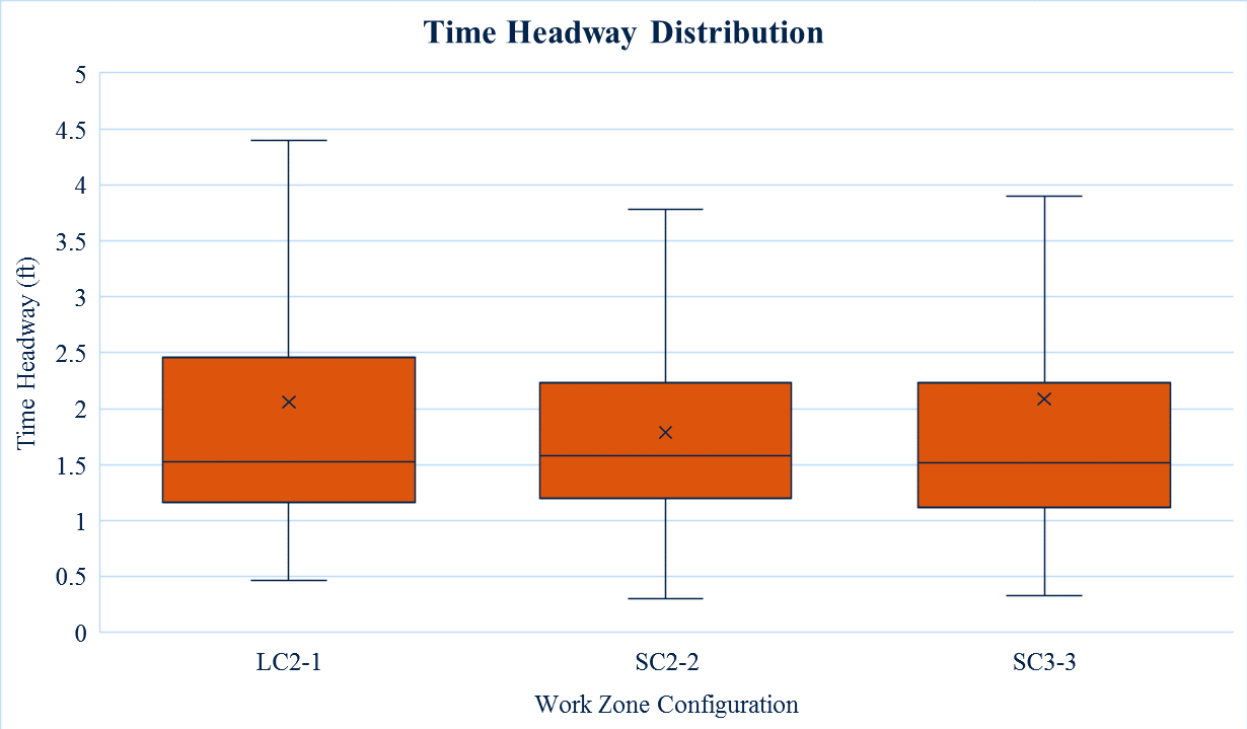

FIGURE 20. TIME HEADWAY DISTRIBUTION AT LC 2-1, SC 2-2, AND SC 3-3

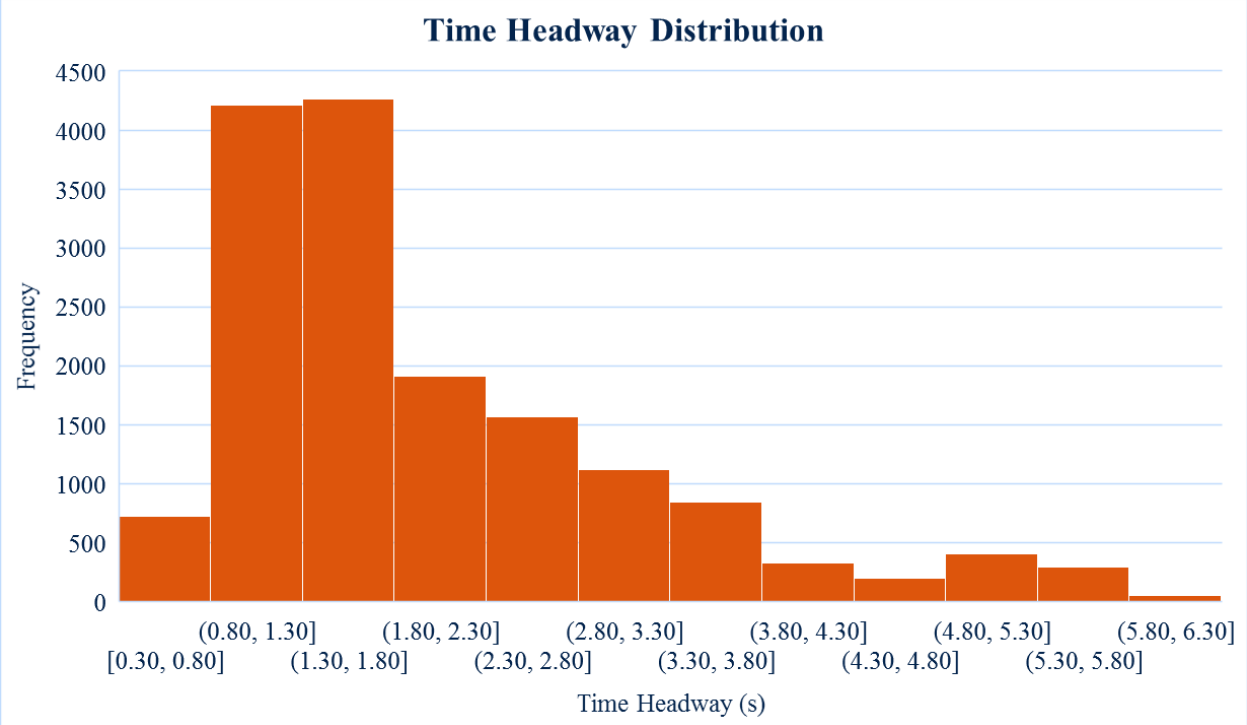

FIGURE 21. TIME HEADWAY DISTRIBUTION

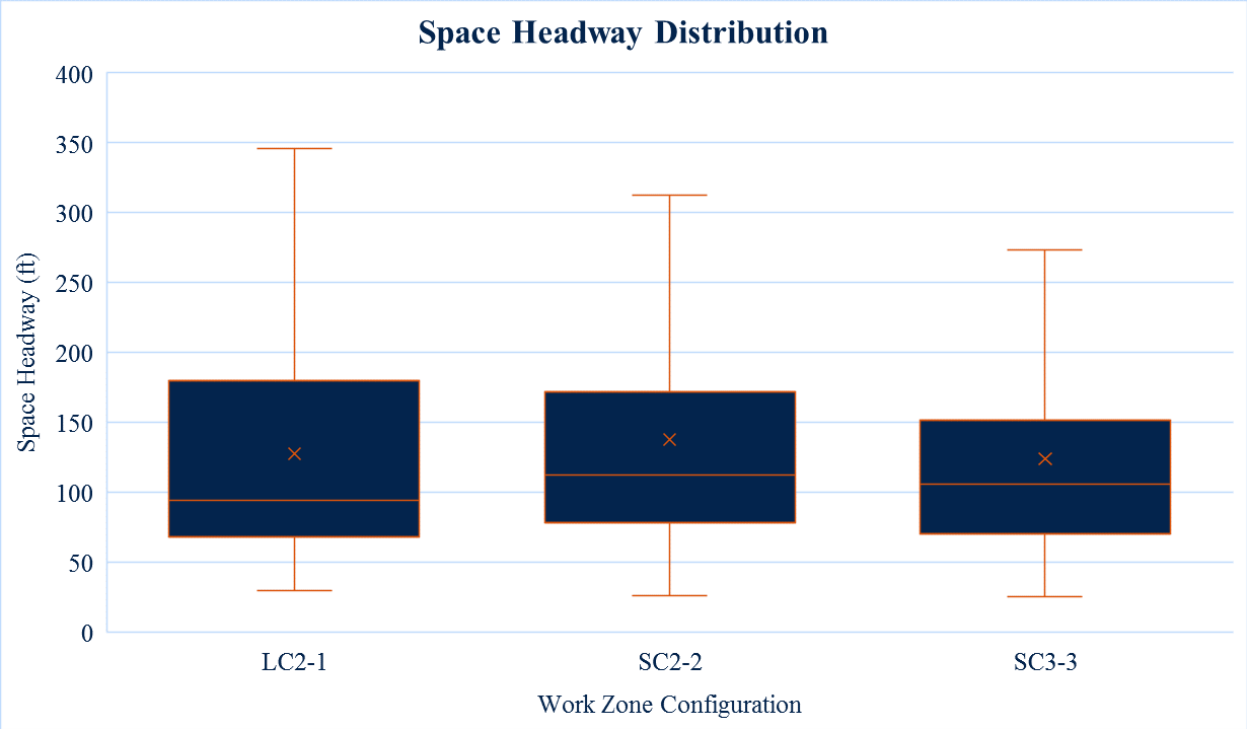

FIGURE 22. SPACE HEADWAY DISTRIBUTION AT LC 2-1, SC 2-2, AND SC 3-3

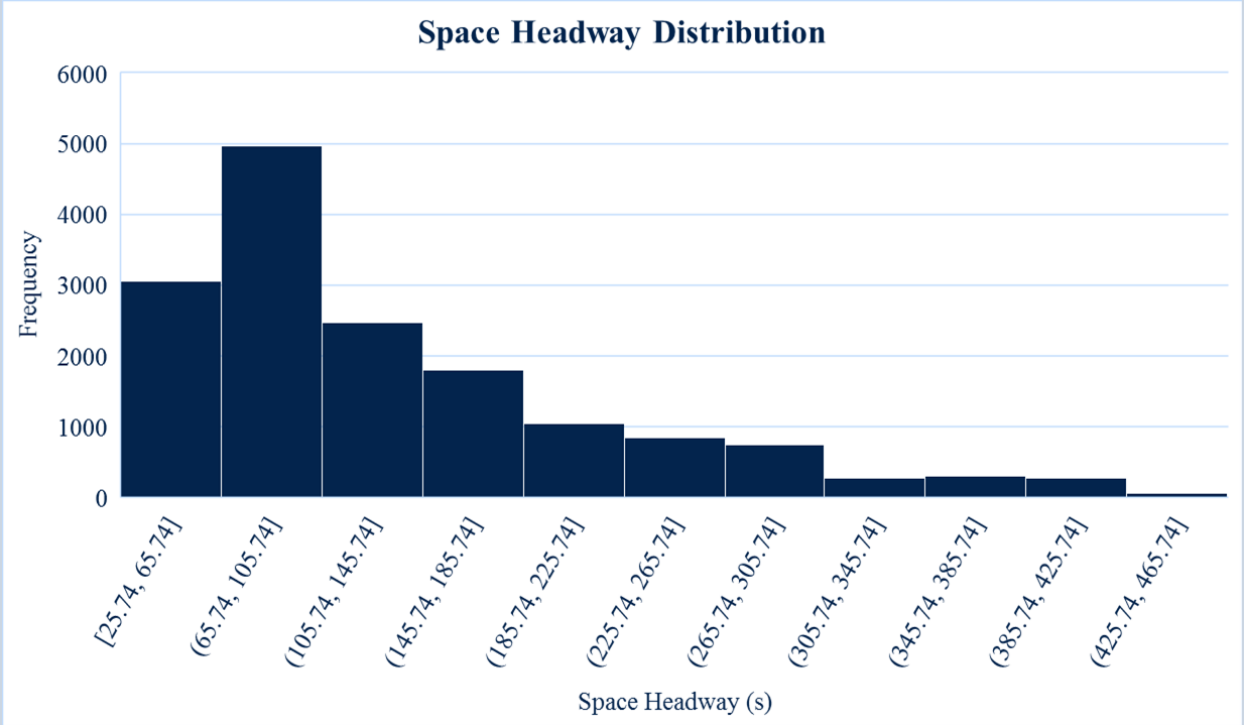

FIGURE 23. SPACE HEADWAY DISTRIBUTION

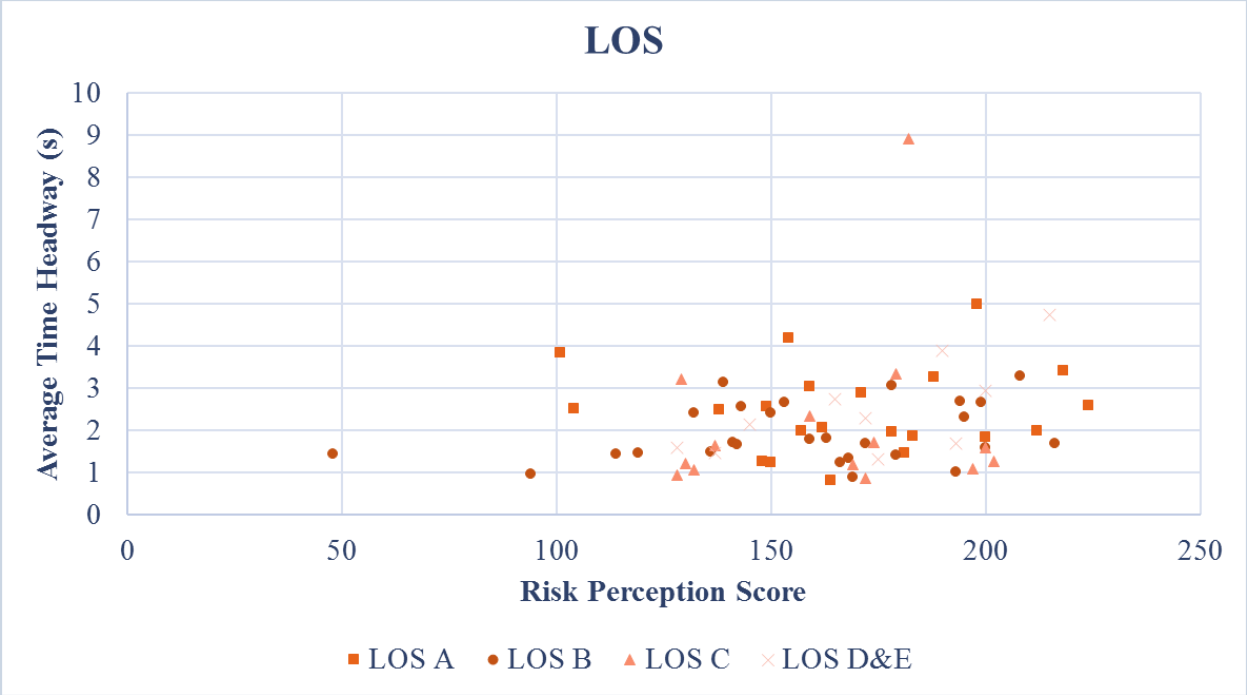

FIGURE 24. AVERAGE TIME HEADWAY AND RISK PERCEPTIONS AT DIFFERENT LOS

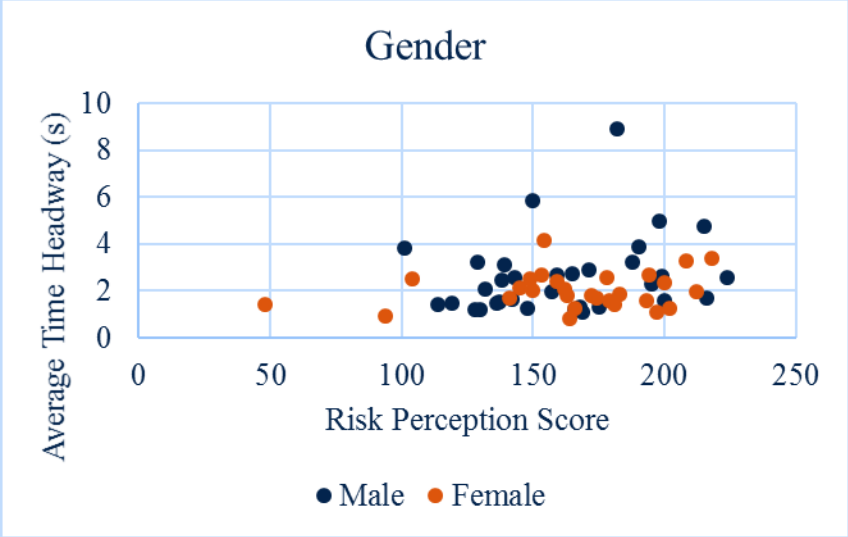

FIGURE 25. AVERAGE TIME HEADWAY AND RISK PERCEPTIONS OF MALE AND FEMALE DRIVERS

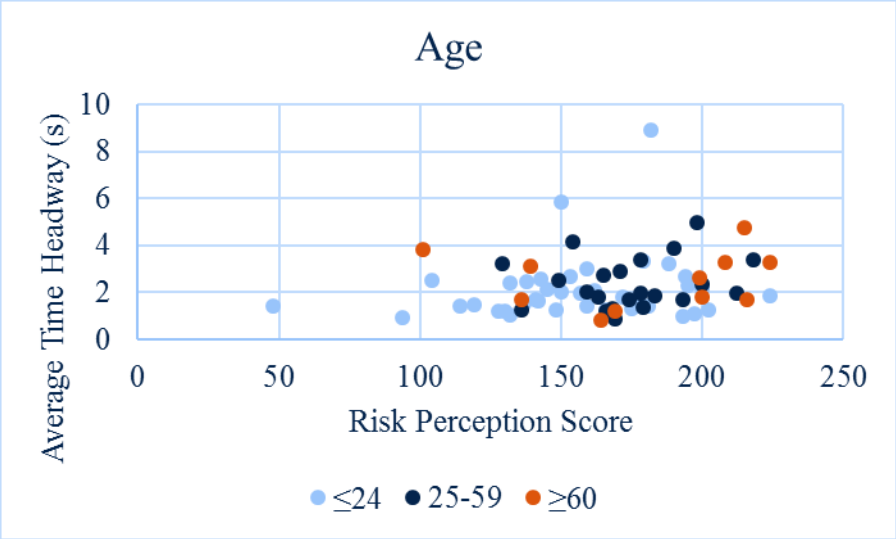

FIGURE 26. AVERAGE TIME HEADWAY AND RISK PERCEPTIONS OF DIFFERENT AGE GROUP

9.3 Appendix C – Summary of Accomplishments

Date	**Type of Accomplishment** *(select from drop down list)*	**Detailed Description** *Provide name of person, name of event, name of award, title of presentation, location and any links to announcements if available.*
May 8, 2019	Conference Presentation	Invited to present at the SHRP 2 Safety Data Oversight Committee (SDOC) meeting
June 8, 2019	Conference Presentation	Invited to present at the Alabama Section Institute of Transportation Engineers (ALSITE) 2019 Annual Meeting
November 1, 2019	Conference Presentation	Accepted for presentation at the Annual Meeting of Transportation Research Board in January 2020
	Choose an item.	
	Choose an item.	
	Choose an item.	